Title
A Compact CO2 Amplifier Optically Pumped by a Tunable 4.3 ﬀm Fe:ZnSe Laser

Author
Tovey, Dana

Publication Date
2021

Peer reviewed|Thesis/dissertation

UNIVERSITY OF CALIFORNIA

Los Angeles

A Compact CO_2 Amplifier Optically Pumped by a Tunable 4.3 μm Fe:ZnSe Laser

A thesis submitted in partial satisfaction

of the requirements for the degree of Master of Science

in Electrical & Computer Engineering

by

Dana Thomas Tovey

2021

ABSTRACT OF THE THESIS

A Compact CO_2 Amplifier Optically Pumped

by a Tunable 4.3 μm Fe:ZnSe Laser

by

Dana Thomas Tovey

Master of Science in Electrical & Computer Engineering

University of California, Los Angeles, 2021

Professor Chandra J. Joshi, Chair

There is currently an ongoing worldwide effort to develop long-wave infrared (8-14 μm) sources with GW-level peak powers and ~1 kHz repetition rate for HHG generation as well as TW-level peak powers for particle acceleration and for long-distance atmospheric propagation. CO_2 lasers can store a great deal of energy and have been demonstrated to amplify 9-10 μm picosecond pulses to very high peak powers. However, the electric discharge typically used for pumping limits these systems to low repetition rates and small aperture beams because of the complexity of the large-scale high-voltage devices used for pumping and the difficulty in maintaining a stable discharge across large apertures at the high pressures (>10 atm) required for short pulse amplification. In principle, optically pumped CO_2 lasers offer a compact alternative without these limitations, but the historic lack of high-energy pump sources at the appropriate wavelength has inhibited the study of picosecond pulse amplification in such a gain medium.

In this thesis, we first present a detailed analysis of 10 μm lasing and gain dynamics in a CO_2 medium optically pumped at ~4.3 μm by a continuously tunable Fe:ZnSe laser system. We then show that lasing can be achieved in a 6 cm long CO_2-He cell at total pressures up to 15 atm by tuning the pump wavelength far from the peak of CO_2 absorption. The optimization of experimentally measured CO_2 vibrational temperatures allows optical-to-optical conversion efficiencies of up to 30% to be reached at atmospheric pressures, falling to ~5% at pressures above 10 atm. At these high pressures, the gain lifetime is measured to be ~1 μs, indicating the possibility of building both multi-pass and regenerative amplifiers using an optically pumped CO_2 medium. Numerical simulations based on density matrix formalism confirm that the amplification of a 3 ps pulse and a sub-picosecond pulse to GW-level powers is feasible in such a compact high-pressure optically pumped CO_2 amplifier.

The thesis of Dana Thomas Tovey is approved.

Benjamin S. Williams

Chee Wei Wong

Chandra J. Joshi, Committee Chair

University of California, Los Angeles

2021

Dedication

To my family and friends, thank you for your unwavering support and interest.

Table of Contents

1 Introduction 1

2 Theory 5

3 Fe:ZnSe pump laser 12

4 Optically pumped CO_2 active medium 14

4.1 Low-pressure lasing 16

4.2 Gain dynamics 18

4.3 High-pressure lasing 23

4.4 Gain lifetime 27

4.5 Lasing in indirectly pumped CO_2 29

4.6 Possibility of repetition rate scaling 30

5 Simulation results 32

5.1 Direct amplification of a 3 picosecond pulse 35

5.2 Chirped-pulse amplification of a sub-picosecond pulse 36

6 Conclusion 38

List of Figures

1 The CO_2 gain spectrum at total pressures of 1 atm (blue) and 20 atm (gray). The black curve indicates the bandwidth of a transform-limited 1 ps pulse centered at 10.28 μm. 1

2 Optical pumping scheme for (a) direct excitation of CO_2 and (b) indirect excitation of CO_2 via CO. 2

3 A simplified energy band diagram of the CO_2 molecule, with the three vibrational modes represented by columns as labeled. 6

4 The gain envelope of the regular 10 μm P branch of CO_2 transitions at a translational temperature of 300 K. Red diamonds indicate the rovibrational lines on which small signal gain was measured in experiment. 8

5 (a) Normalized population of CO_2 molecules in each energy level of the asymmetric mode when calculated with a Treanor distribution function (in red) and a Boltzmann distribution function (in blue) for T_3 temperatures of 1800 K (top) and 4200 K (bottom). (b) The normalized gain spectrum for a gas mixture of 1 atm CO_2 and 19 atm He, optically pumped to a T_3 value of 4200 K. 10

6 (a) A simplified schematic of the Fe:ZnSe MOPA system. (b) The Fe:ZnSe master oscillator. 12

7 (a) Output energy of the Fe:ZnSe MOPA as a function of wavelength for the (i) master oscillator, (ii) MOPA system at full pump energy without absorbing element between MO and PA, (iii) MOPA system at full pump energy with absorber, and (iv) MOPA system at reduced pump energy without absorber. (b) Typical temporal pulse profiles for (i) the 2.94 μm Er:YAG pump laser, (ii) the master oscillator, and (iii) the MOPA output. 13

8 Experimental setup of the optically pumped CO_2 laser. DM – dichroic mirror, the left DM can be replaced by a diffraction grating. 15

9 (a) The amount of 10 μm energy generated in the optically pumped CO_2 laser as a function of absorbed pump energy. A least squares linear fit to the aggregate data is shown in black. (b) Optical-to-optical conversion efficiency in the optically pumped CO_2 laser for a pump wavelength of 4.23 μm. The black curve indicates a least squares parabolic fit to the data. 17

10 (a) The asymmetric stretching mode vibrational temperature T_3 and (b) the translational temperature T within a cell of 50 torr pure CO_2 optically pumped at 4.3 μm as a function of time. The blue curves show the results of raw data; the red curves show this data with a 50 point moving average filter applied to reduce noise. The pump pulse temporal profile is shown in black. 19

11 (a) The asymmetric stretching vibrational mode temperature T_3 and (b) the corresponding peak gain coefficient in an optically pumped CO_2 active medium vs. absorbed 4.3 μm pump energy per volume. Each color corresponds to a different amount of pure CO_2. Experimental measurements are shown in diamonds. 21

12 The peak asymmetric stretching vibrational mode temperature, T_3, in an optically pumped CO_2 active medium as a function of total pressure for pure CO_2 (see blue curve) and for dilute CO_2 mixtures (see red curve). 22

13 (a) Normalized absorption in 0.75 atm CO_2 and 9.25 atm He. Red markers indicate pump wavelengths used in experiment. (b) Maximum lasing pressure vs estimated experimental absorption coefficient. Numbers correspond to pump wavelengths

indicated in (a). The green star indicates maximum lasing pressure after increasing the pump intensity by a factor of ~2 to ~5.3 MW/cm^2. 24

14 Beam profiles of (a) the 4.4 μm pump laser and (b) the 10.6 μm optically pumped CO_2 laser output at a total pressure of 15 atm. 25

15 (a) Optical-optical conversion efficiency of the optically pumped CO_2 laser as a function of pressure using three different output couplers. (b) Conversion efficiency as a function of cavity Q factor at three different pressures. (c) 10 μm lasing energy generated vs. 4.40 μm pump energy absorbed at 7 atm total pressure. 26

16 The 4.40 μm pump pulse (blue) and the amplification factor of the 10.6 μm probe pule (red) as a function of time for a gas mix of 0.75 atm CO_2 and 10.25 atm Helium. 27

17 (a) Total amplification of the 10.6 μm probe pulse in the 6 cm optically pumped CO_2 cell and (b) gain lifetime as a function of total pressure. 28

18 (a) Normalized absorption in 1 atm CO. Red markers indicate pump wavelengths used in experiment. (b) Maximum lasing pressure vs estimated experimental absorption coefficient. Numbers correspond to pump wavelengths indicated in (a). 30

19 (a) Deflected probe signal (in blue) and Fe:ZnSe pump pulse (in red). (b) Deflected probe signal and recovery. The dashed white line indicates an exponential fit with a time constant of 0.33 ms. 31

20 (a) The gain spectrum of an active medium comprised of 1 atm CO_2 (63% $^{12}C^{16}O_2$ isotopologue, 37% $^{13}C^{16}O_2$) and 19 atm He, pumped to a T_3 value of 3300 K. The dashed black line shows the frequency spectrum of a 500 fs seed pulse centered at 10.7 um. (b) The normalized gain spectrum of an active medium comprised of 1 atm CO_2

(21% $^{12}C^{16}O_2$, 43% $^{12}C^{18}O_2$, and 36% $^{12}C^{16}O^{18}O$ isotopologue) and 19 atm He. A total bandwidth of ~3 THz centered around 9.3 μm wavelength is achieved. 33

21 Simulation results for the amplification of a 3 ps pulse centered at 10.29 μm in a gas mix of 1 atm CO_2 and 19 atm He optically excited to a T_3 value of 4200 K. (a) The temporal profile of the pulse before (top) and after (bottom) amplification. (b) The pulse energy as a function of amplifier length, discounting losses due to propagation or output coupling. 36

22 Simulation results for the amplification of a sub-ps pulse in an optically pumped CO_2 amplifier comprised of 1 atm CO_2 (63% $^{12}CO_2$, 37% $^{13}CO_2$) and 19 atm He. The temporal profile of the pulse before stretching (see top), after amplification (see middle), and after compression (see bottom) are shown on the left. The frequency spectrum of the pulse at each stage is shown on the right. 50% loss of energy during compression is assumed. 37

Acknowledgements

I would like to thank Dr. Sergei Tochitsky for introducing me to the world of photonics and guiding me through every step of this project, and I would like to thank Professor Chan Joshi for his constant support and inspiring dedication to science. I would also like to thank Dr. Jeremy Pigeon for his essential assistance in running these experiments, and I would like to thank Dr. Pigeon, Eric Welch, and Daniel Matteo for their thoughtful answers to my many questions and for making the lab a more enjoyable place to learn. Finally, I would like to thank Dr. Mikhail Polyanskiy from Brookhaven National Laboratory for his assistance in running simulations.

This work was supported by the Office of Naval Research (ONR) MURI grant No. N00014-17-1-2705 and the Department of Energy (DOE) Office of Science Accelerator Stewardship Award No. DE-SC0018378.

1 Introduction

Picosecond and subpicosecond pulses with TW-level power in the long-wave infrared region (8-14 μm) are desirable for the study of high-field physics and nonlinear optics in this region of high atmospheric transmission [1-4]. At present, high-pressure CO_2 laser systems are the only viable candidate for generating such pulses, because the CO_2 molecule is capable of storing tens of Joules of energy in a large volume for 10 μm amplification and does not face the damage threshold limitations that inhibit an optical parametric amplifier from reaching high peak powers at these wavelengths. In addition, while the individual rovibrational transitions of the CO_2 gain spectrum have a relatively narrow bandwidth, these transitions can be broadened via collisions at high pressures to overlap with one another and provide the THz bandwidth necessary for picosecond pulse amplification (see Figure 1). CO_2 lasers have been used to amplify 10 μm pulses as short as a few ps [5-7]. Recently, powers as high as 15 TW have been achieved using CO_2 lasers in a master-oscillator power-amplifier (MOPA) system at the UCLA Neptune Laboratory [6], and 5

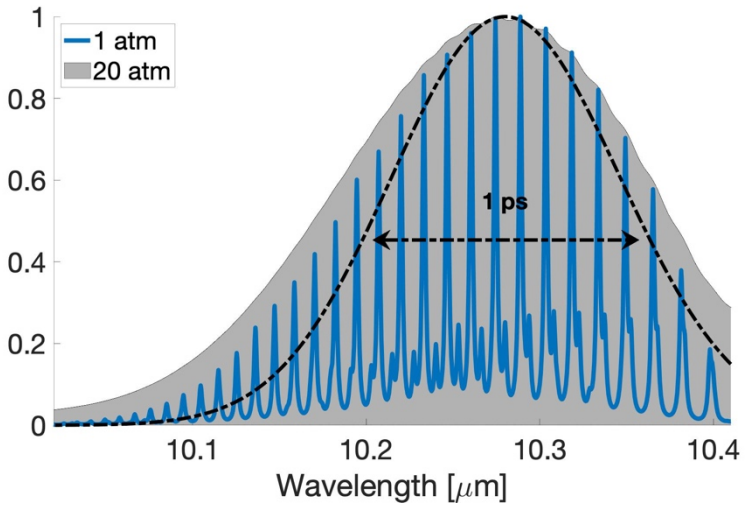

Figure 1. The CO_2 gain spectrum at total pressures of 1 atm (blue) and 20 atm (gray). The black curve indicates the bandwidth of a transform-limited 1 ps pulse centered at 10.28 μm.

TW, 2 ps pulses have been generated using CO_2 amplifiers at the Accelerator Test Facility (ATF) at Brookhaven National Laboratory [7]. CO_2 laser systems are typically pumped with an electric discharge, however, and the voltage required for breaking the gap between electrodes scales linearly with pressure. As a result, at the high pressures (>10 atm) needed for a smooth broadband gain spectrum, it is extremely difficult to maintain a stable electric discharge in large volumes, and repetition rates are limited.

In principle, the CO_2 active medium can be excited optically to circumvent this discharge pressure limitation. As shown in Figure 2(a), a pump source at ~4.3 μm can be used to directly populate the upper laser level 001 of the 10 μm laser channel and excite the entire asymmetric stretching mode of the CO_2 molecule, while the lower laser level 100 remains only weakly thermally populated. Optical pumping of a CO_2 laser was historically first demonstrated using an incoherent CO-air flame to excite CO_2 at ~4.3 μm, producing ~1 mW of cw radiation at 10.6 μm [8]. Later, several groups explored the potential of optically pumping a high-pressure CO_2 laser, which would exhibit continuous spectral tuning across the broad gain bandwidth. One such group demonstrated lasing in optically pumped CO_2 at a total pressure of 33 atm using a pulsed ~4.23

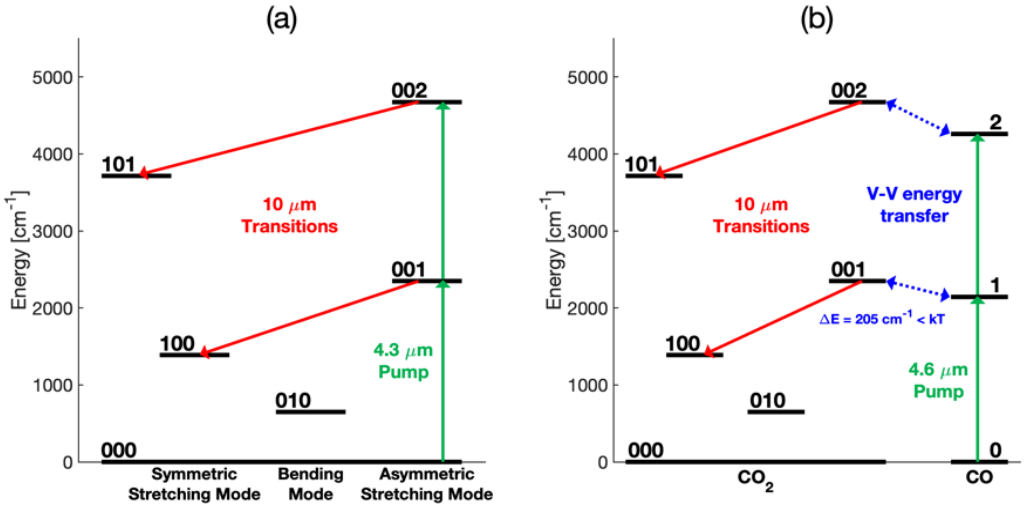

Figure 2. Optical pumping scheme for (a) direct excitation of CO_2 and (b) indirect excitation of CO_2 via CO.

μm HBr laser for pumping, but optical-to-optical conversion efficiency was not optimized or reported [9]. In addition, the gain length was restricted to only ~1 mm due to the extremely high absorption coefficient and short gain lifetime at such high pressures. This reduced the cavity round-trip time but also decreased the single-pass gain in such a short CO_2 cell. The 101 level of the CO_2 molecule has also been pumped using a ~2.7 μm HF chemical laser [10,11], but this method was not pursued beyond the initial experimental demonstration, as the fast collisional decay of the 101 level simultaneously populates both the upper (001) and lower (100) laser levels for the 10 μm band. In general, the lack of available energetic pump sources operating at wavelengths that are efficiently absorbed by CO_2 has prevented the demonstration of high gain in a high-pressure optically pumped CO_2 amplifier.

An alternative optical pumping scheme has also been explored, in which a partner molecule is resonantly excited by optical pumping and the absorbed energy is then transferred to CO_2 via collisions. This method enables the use of pump wavelengths that do not overlap directly with CO_2 absorption lines and can also result in significantly longer gain lifetimes due to the slow exchange of vibrational energy between different molecules such as N_2O and CO. Figure 2(b) depicts such a scheme using CO as the collisional partner molecule to be optically excited. The small quantum defect between the first vibrational level of CO and the first level of the CO_2 asymmetric stretching mode allows energy to be efficiently transferred from CO to CO_2. Lasing was demonstrated in a CO-CO_2-He mix at a total pressure of 16 atm by pumping CO at 4.8 μm using the second harmonic of a 9.6 μm TEA CO_2 laser [12]. Less than 1 mJ of 10 μm light was generated, however, as this method has faced a similar lack of energetic pump sources.

Recently, significant progress has been made on solid-state lasers using iron-doped zinc chalcogenides to provide tunable sources around 3-5 μm that have the potential to be scaled up to

Joule-class energies [13]. Specifically, the development of an Fe:ZnSe laser system capable of producing ≤60 mJ, 200 ns pulses at a wavelength tunable from 3.8-5.0 μm has provided an energetic pump source for optically exciting CO_2 either directly at ~4.3 μm or indirectly by pumping CO at ~4.6 μm [14]. This has opened a new opportunity for studying the feasibility of generating or amplifying picosecond or sub-picosecond 10 μm pulses in an optically pumped CO_2 active medium, which has never before been thoroughly analyzed.

In this thesis, we present a detailed study of lasing and gain dynamics in a CO_2 active medium optically pumped by such a tunable Fe:ZnSe laser. The thesis will be structured as follows. Chapter 2 will introduce a generally accepted theoretical temperature model that describes an excited CO_2 medium, providing necessary background information for understanding the gain dynamics of a CO_2 laser. Chapter 3 will detail our experimental results, including the demonstration of high gain and high conversion efficiencies in optically pumped CO_2 at atmospheric pressures [15], the optimization of pump wavelength to achieve lasing at total pressures up to 15 atm, and measurements of gain lifetime as a function of pressure [16]. The alternative pumping scheme in which CO_2 is indirectly excited via pumping CO will also be discussed here [16]. We also evaluate experimentally a maximum repetition rate at which a CO_2 medium can be optically pumped by analyzing the dissipation of pressure or heat waves caused by the pump pulse [16]. Chapter 4 will detail theoretical simulations that model the amplification of short pulses in a high-pressure optically pumped CO_2 amplifier [17]. Finally, Chapter 5 will present our conclusions and look forward to future work.

2 Theory

Ultimately, the development of an optically pumped CO_2 laser system capable of generating high power 10 μm pulses requires a detailed understanding of gain dynamics in such an optically excited molecular active medium. The properties of a discharge pumped CO_2 gain medium have been well characterized using a generally accepted temperature model in which each vibrational mode is assigned a vibrational temperature describing the Boltzmann distribution of population in that mode [18-22]. This model can similarly be applied to an optically pumped CO_2 system, as the relationship between the relaxation times of the main kinetic processes occurring in molecular gases remains the same:

$$\tau_{VR} \ll \tau_{VV} \ll \tau_{VV'} \tag{1}$$

where τ_{VR}, τ_{VV}, and $\tau_{VV'}$ are time constants describing the rates at which equilibrium is achieved among rotational energy levels, among vibrational energy levels within a single vibrational mode, and among different vibrational modes of the CO_2 molecule, respectively. Equilibrium is reached among individual rotational levels first – such that the population among these levels can be described according to a Boltzmann distribution with translational or gas temperature, T – on a time scale of $\tau_{VR} \approx 0.2$ ns at 1 atm of pressure [18]. The distribution of population within the different vibrational energy levels in a single vibrational mode reaches a Boltzmann distribution on a time scale of $\tau_{VV} \approx 5$ ns at 1 atm [18]. Equilibrium among different vibrational modes or different gases (e.g. N_2) within a mixture occurs on a much longer time scale of $\tau_{VV'} \leq 1$ μs at 1 atm [18]. This hierarchy of relaxation times in the CO_2 molecule is the main reason for the applicability of this temperature model when considering a typical pump laser pulse on the order

of 100 ns. The population of each vibrational energy level can thus be accurately described using a Boltzmann distribution with a different temperature, T_i, assigned to each vibrational mode i:

$$N_v = N_0 \exp\left(-\frac{hc\nu G_i}{k_B T_i}\right) \tag{2}$$

where N_v is the population of molecules in level v of the mode, N_0 is the population of molecules in the ground state, G_i is the energy gap between levels in vibrational mode i, and h, c, and k_B are the usual physical constants.

The CO_2 molecule has three vibrational modes: symmetric stretching (T_1), bending (T_2), and asymmetric stretching (T_3). Figure 3 shows the vibrational energy levels of interest in a CO_2 laser, with each column corresponding to a distinct vibrational mode. It can be seen that the upper laser levels for 10 μm lasing transitions in CO_2 are energy states corresponding to excitation of the

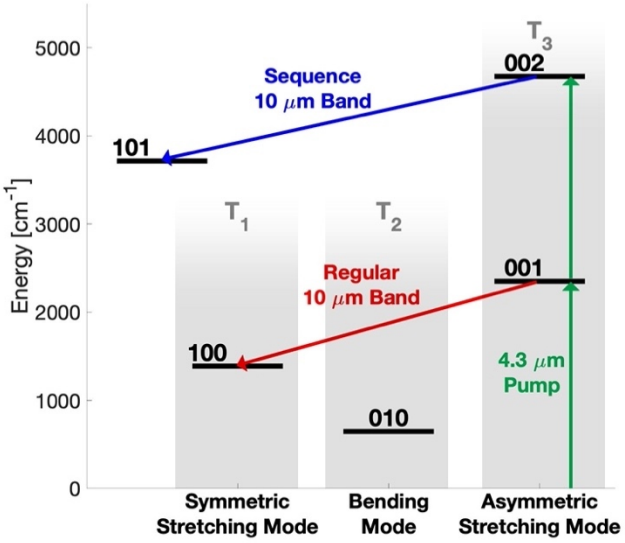

Figure 3. A simplified energy band diagram of the CO_2 molecule, with the three vibrational modes represented by columns as labeled.

asymmetric stretching mode. As a result, optimizing gain in a CO_2 active medium corresponds to maximizing T_3 without increasing T_1 and T_2. In the case of optical pumping with a ~4.3 μm pump source, it is reasonable to assume that all of the absorbed pump energy is stored in this asymmetric stretching mode, while the vibrational temperatures of other modes, T_1 and T_2, tend to remain equal to the translational temperature of the gas, T. As a result, optimization of gain is easier to achieve in an optically pumped CO_2 active medium than in discharge-excited CO_2 systems [19]. This ability to selectively excite the asymmetric stretching mode via the absorption of 4.3 μm pump photons is an additional advantage of pumping CO_2 optically. It has been demonstrated that in an optically pumped CO_2 medium, T_3 values as high as 4200 K have been reached [23], while traditional discharge pumped CO_2 lasers fail to reach T_3 values above 1800 K [18].

For optical excitation, the population of molecules in each individual energy level can be determined with knowledge of the translational temperature, T, and this vibrational temperature, T_3. Full characterization of an optically pumped CO_2 gain medium can thus be achieved by making time-resolved measurements of both T and T_3. The translational temperature can be calculated from measurements of small signal gain on multiple different regular band transitions. Figure 4 shows the envelope of the 10P branch of the normalized CO_2 gain spectrum as a function of rotational quantum number j at an example temperature of T = 300 K. The shape of this envelope depends on the translational temperature since the population of molecules in a particular rotational-vibrational state vj is given by [18]:

$$N_{vj} = N_v \left(\frac{2hcB_v}{k_B T}\right)(2j+1)\exp\left(-\frac{hc}{kT}[B_v j(j+1) - D_v j^2(j+1)^2]\right) \qquad (3)$$

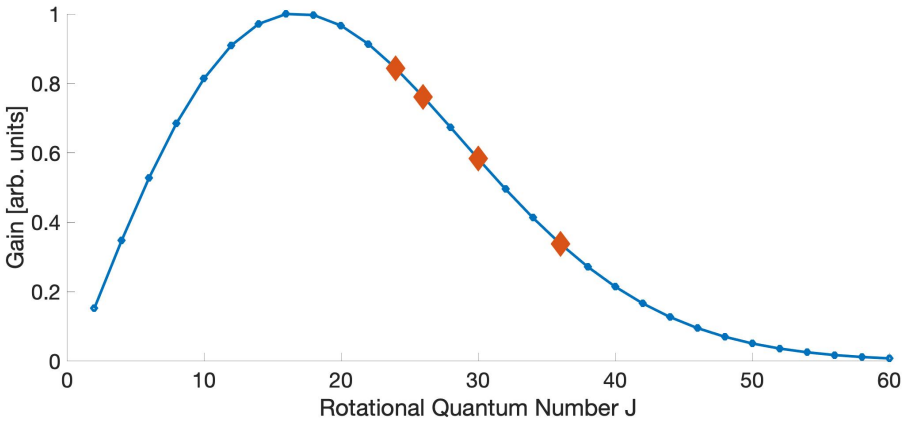

Figure 4. The gain envelope of the regular 10 μm P branch of CO_2 transitions at a translational temperature of 300 K. Red diamonds indicate the rovibrational lines on which small signal gain was measured in experiment.

where v refers to the specific vibrational state (for example, 001), N_v is the population of molecules in the vibrational state as a whole (given in Equation 2), B_v and D_v are rotational constants for the particular vibrational state, and j is the rotational quantum number [23]. The translational temperature T can thus be found by fitting a curve to experimentally measured small-signal gain values on various 10P CO_2 lines. Analysis of this method of calculating T revealed that the slope of the curve on the high-j side of the peak of the gain distribution is very sensitive to changes in temperature. Chapter 4.2 will discuss our experimental measurements of T as a function of time using this method; we chose to measure gain on the 10P(24), 10P(26), 10P(30), and 10P(36) rovibrational transitions (see Figure 4) to maximize our temperature measurement accuracy. The accidental overlap between regular band lines (001-100) and sequence band (002-101) or hot band (011-110) lines was also considered when choosing rovibrational lines, as these overlaps can distort the gain envelope and introduce additional error in the measurement of T [24,25].

The asymmetric stretching mode temperature, T_3, can be calculated from measurements of small signal gain on both a regular band transition and a sequence band transition using the following relation [18,23]:

$$\frac{g_{\mathrm{seq}}}{g_{\mathrm{reg}}} = 2\exp\left(-\frac{hcG_3}{k_B T_3}\right) \tag{4}$$

which gives:

$$T_3 = \frac{hcG_3}{k_B \ln\left(\frac{2g_{\mathrm{reg}}}{g_{\mathrm{seq}}}\right)} \tag{5}$$

where g_{seq} is the small signal gain on a sequence band transition (002-101), and g_{reg} is the small signal gain on a regular band transition (001-100) with an equivalent rotational quantum number j. This equation, however, assumes a perfect Boltzmann exponential distribution of population in the asymmetric stretching mode of CO_2. Previous experiments have indicated that for the very high values of T_3 that can be achieved with optical pumping, the distribution of population in the asymmetric mode can be more accurately described using a Treanor distribution function [23,26]:

$$N_{00n} = N_0 \exp\left(-\frac{hc}{k}\left(\frac{nG_1}{T_3} - \frac{n(n-1)w_e x_e}{T}\right)\right) \tag{6}$$

where N_{00n}, N_0, and G_1 are defined above, and $w_e x_e$ is the anharmonicity constant introduced in this formula. This arises from the fact that the Boltzmann distribution is based on the assumption

that all vibrational levels in a single mode are evenly spaced. In reality, the separation between levels in the CO_2 asymmetric stretching mode is not constant but rather decreases for higher levels, resulting in a slightly less efficient exchange of energy between these levels and therefore a distribution of energy that is not perfectly exponential.

Calculations have been performed to determine whether this change in distribution function plays a significant role for an optically pumped CO_2 medium. Figure 5(a) displays the normalized population in each 00n energy level of CO_2 when calculated using a Boltzmann distribution and a Treanor distribution for T_3 values of 1800 K and 4200 K. Recall that these two values correspond to the respective temperatures that are typically reached when pumped by electric discharge and

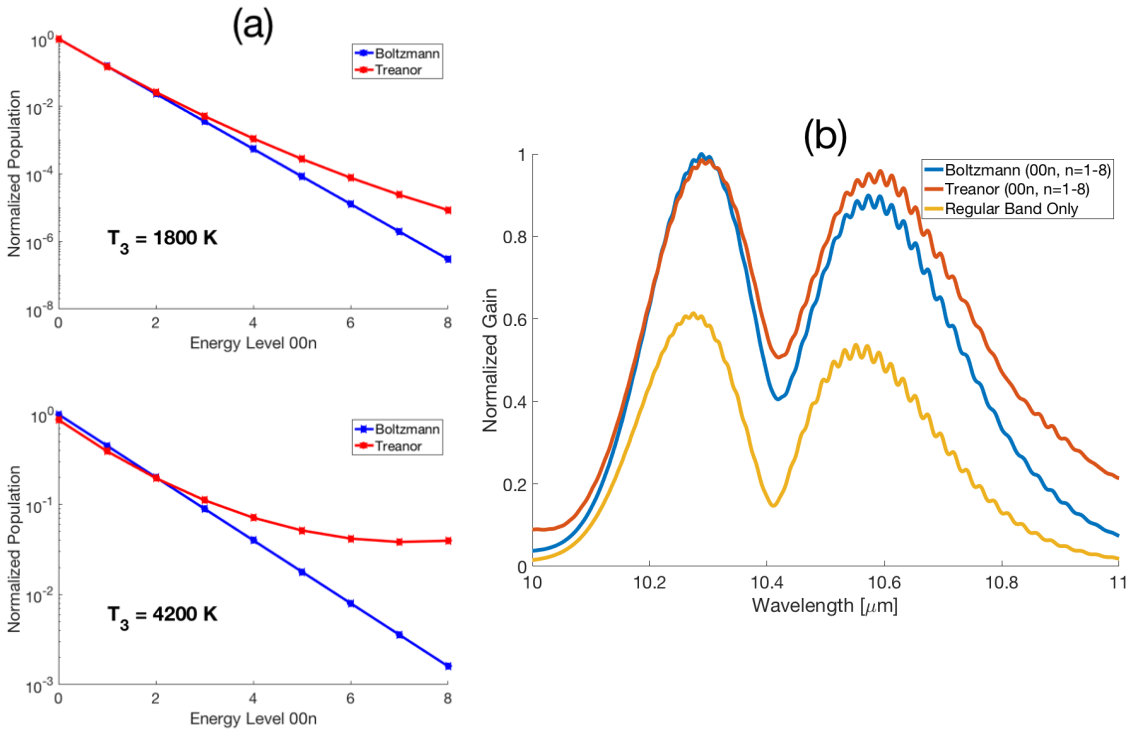

Figure 5. (a) Normalized population of CO_2 molecules in each energy level of the asymmetric mode when calculated with a Treanor distribution function (in red) and a Boltzmann distribution function (in blue) for T_3 temperatures of 1800 K (top) and 4200 K (bottom). (b) The normalized gain spectrum for a gas mixture of 1 atm CO_2 and 19 atm He, optically pumped to a T_3 value of 4200 K.

that can be reached when pumped optically. It is apparent that, in comparison with the Boltzmann distribution function, the Treanor distribution function places a significantly greater portion of the total population in the 00n energy levels for n > 3, increasing the gain present on upper sequence bands (00n-10(n-1)). It should be noted that while these bands are red-shifted due to anharmonicity, the transition frequencies of their R and P branches are relatively close to that of the regular band (<100 MHz difference) and are therefore still involved in the amplification process for the case of picosecond pulses. Figure 5(b), which displays the normalized gain spectrum around 10 μm for a 20 atm CO_2-He gas mix (containing 1 atm pure CO_2) that has been optically excited to a T_3 value of 4200 K, illustrates how sequence bands (00n-10(n-1)) contribute to the overall gain spectrum. The yellow curve represents gain on the regular band transitions, excluding extra gain from the sequence bands discussed above. The blue and red curves represent the gain spectrum with all sequence bands included when determining the asymmetric mode level populations using a Boltzmann distribution function and Treanor distribution function, respectively.

The yellow gain curve depicted in Figure 5(b) demonstrates that sequence band transitions have a significant contribution to the overall gain spectrum in a highly excited CO_2 gain medium. The red and blue curves show that the difference in peak gain at high pressures when calculated using a Treanor function in place of a Boltzmann function is negligible for realistic T_3 values at high pressures. It should be noted that the use of a Treanor function instead of a Boltzmann function to model population only substantially affects higher levels and sequence bands. As a result, using the Treanor function does slightly red-shift the wavelength at which gain is maximized, but the overlap between sequence band and regular band rovibrational lines at high pressures eliminates any significant disparity. Because differences in the gain spectrum at high

pressures using different population distributions are negligibly small (see Figure 5(b)), the remainder of this thesis uses a Boltzmann function to describe population and to measure T_3.

3 Fe:ZnSe pump laser

The experiments discussed in the following chapter of this thesis were performed using a Fe:ZnSe MOPA system for optically pumping a CO_2 gain medium [14]. A simplified schematic of this system is shown in Figure 6(a). A flashlamp-pumped, Q-switched 2.94 μm Er:YAG laser producing ~200 ns pulses of ~250 mJ of energy is used to pump the system, with the 2.94 μm pulse being split in multiple ways to pump both the oscillator and the three power amplifiers as shown. A diffraction grating within the Fe:ZnSe master oscillator laser cavity allows for continuous tuning over a wavelength range of 3.8-5.0 μm. A picture of this master oscillator with the diffraction grating, Fe:ZnSe crystal, and Er:YAG pump laser labeled is shown in Figure 6(b). It should be noted that because the Fe:ZnSe gain spectrum is peaked at ~4.15 μm, the gain medium will produce broadband amplified spontaneous emission centered at ~4.15 μm when the master oscillator is tuned to operate at long wavelengths >4.6 μm. As a result, while this did not affect

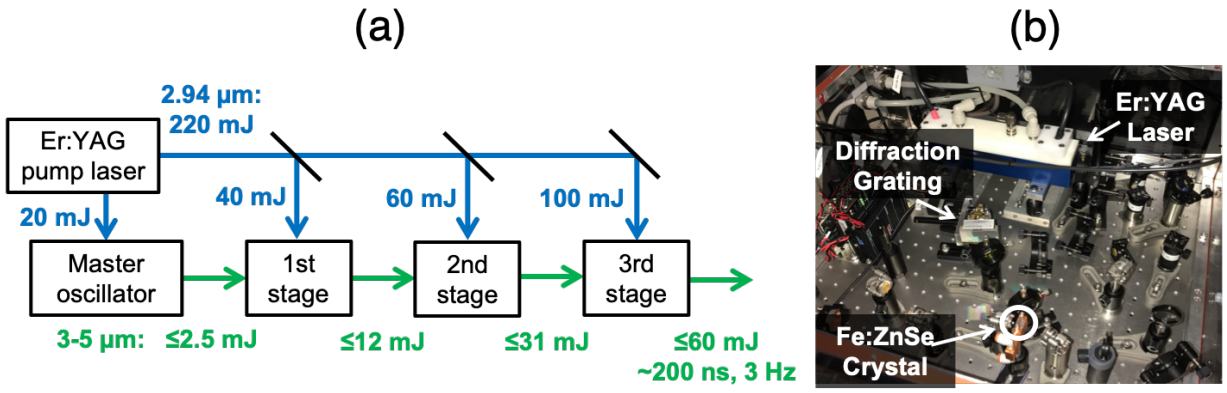

Figure 6. (a) A simplified schematic of the Fe:ZnSe MOPA system. (b) The Fe:ZnSe master oscillator.

our operation of the Fe:ZnSe laser for pumping CO_2 at ~4.3 μm, studying the indirect pumping scheme in which CO is optically pumped at ~4.6 μm required the introduction of an unpumped Fe:ZnSe crystal as an absorbing element between the master oscillator and power amplifier to eliminate this parasitic self-lasing [14].

Figure 7(a) shows measurements of pulse energy as a function of output wavelength under different pumping conditions. The black curve shows the tuning curve of the master oscillator, multiplied by 4 for visibility. The black, red, and blue markers show the tuning curve of the MOPA system at full pump energy without any absorbing element, at full pump energy with the absorbing element, and with reduced pump energy without any absorbing element, respectively. For the low pressure optically pumped CO_2 experiments discussed in Chapters 4.1-4.2, only the master oscillator with pulse energies of ≤2.5 mJ was used for pumping CO_2, as the power amplifier system had not yet been fully developed [27]. For the high-pressure experiments discussed in Chapters

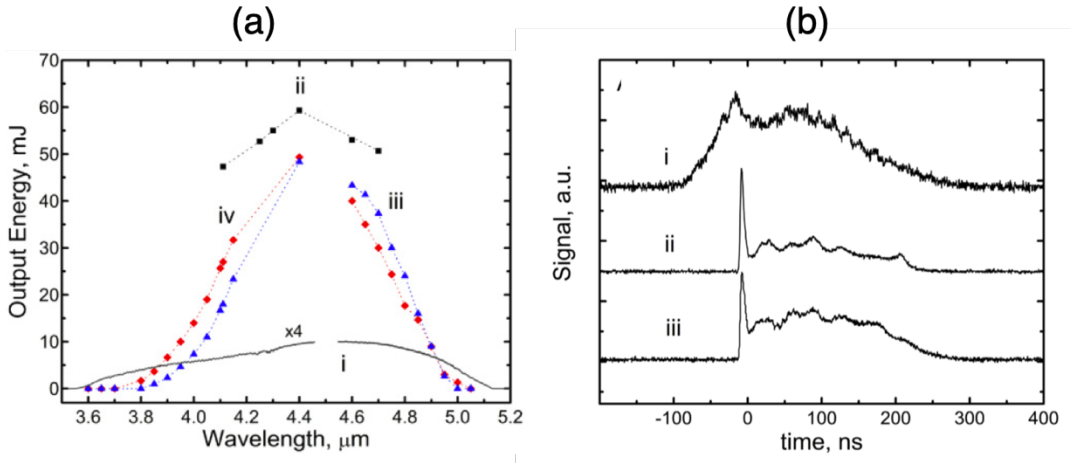

Figure 7. (a) Output energy of the Fe:ZnSe MOPA as a function of wavelength for the (i) master oscillator, (ii) MOPA system at full pump energy without absorbing element between MO and PA, (iii) MOPA system at full pump energy with absorber, and (iv) MOPA system at reduced pump energy without absorber. (b) Typical temporal pulse profiles for (i) the 2.94 μm Er:YAG pump laser, (ii) the master oscillator, and (iii) the MOPA output.

4.3-4.6, the full MOPA system was utilized, with the absorbing element put in place for the indirect pumping scheme results discussed in Chapter 4.5. Figure 7(b) shows typical temporal profiles for the 2.94 μm Er:YAG pump laser, the master oscillator, and the entire MOPA system. Further details on this system can be found elsewhere [14].

4 Optically pumped CO_2 active medium

Experimental measurements of lasing and small-signal gain in an optically pumped CO_2 medium were all performed using a similar experimental setup, which is shown in Figure 8. The green arrows indicate the optical path of the Fe:ZnSe pump laser. A NaCl wedge angled at 45 degrees was used to sample ~1% of the pump pulse to diagnose the input pump energy prior to reaching the CO_2 cell as shown. For all experiments discussed in this chapter, the entire experimental area was purged with N_2 or Ar gas to eliminate any absorption of the pump pulse by CO_2 in the ambient air.

For lasing experiments, the laser cavity was formed by two curved dichroic mirrors surrounding a gas cell sealed with Brewster-angled NaCl windows. The dichroic mirrors are 99.5% reflective at ~10.6 μm and 99% transmissive at ~4.3 μm and have a radius of curvature of 70 cm. Low-pressure lasing measurements were performed using a 25 cm long cell; high-pressure lasing measurements where CO_2 absorption was stronger were performed using a 6 cm long cell. For all measurements, the cavity length was ~50 cm. The 10.6 μm laser radiation decoupled through the downstream (leftmost in Figure 8) dichroic mirror was measured as shown. A 10 μm narrow-bandpass filter was used to eliminate any residual 4.3 μm pump radiation. As indicated in Figure 8, one of the dichroic mirrors could be replaced with a diffraction grating to vary the cavity Q

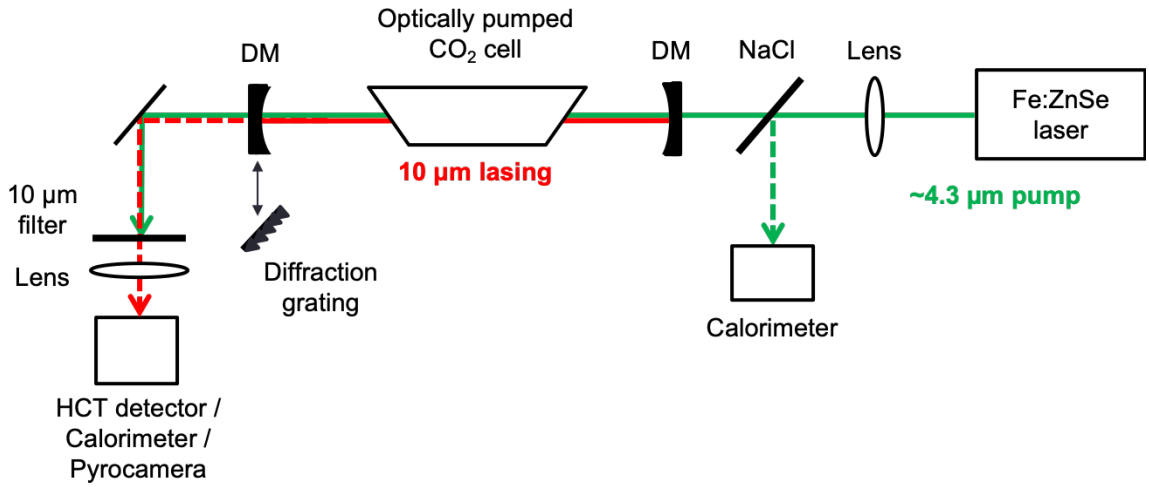

Figure 8. Experimental setup of the optically pumped CO_2 laser. DM – dichroic mirror, the left DM can be replaced by a diffraction grating.

factor. For this configuration, the zeroth order of the grating was used to decouple radiation out of the cavity. Two different diffraction gratings were used in this study, with measured reflectivities of ~71% and ~97.7% at 10.6 µm and groove densities of 135 gr/mm and 150 gr/mm, respectively.

To measure small-signal gain, the left dichroic mirror was removed, and a commercial, low-pressure, discharge-pumped, pulsed CO_2 laser was used to probe the active medium. Typical probe pulses contained a few mJs of energy and consisted of a short (~100 ns) spike followed by a long (>20 µs) tail. Measurements were performed on the tail of the pulse such that the probing peak power was only a few Watts, far below gain saturation.

For the low-pressure gain measurements on both the regular and sequence bands described in Chapter 4.2, the 97.7% reflective diffraction grating was placed in a non-Littrow configuration within the probe laser cavity such that this probe laser pulse is doubly diffracted. The probe laser cavity length of ~1 m and this double passing through the diffraction grating increased dispersion to allow for precise tuning of the probe laser on individual rovibrational transitions of both the regular and sequence 10 µm branches of CO_2 [28]. Recall from Chapter 2 that measuring gain on

several rovibrational transitions allows for time-dependent measurements of the vibrational mode temperatures in a CO_2 active medium. To maximize the Q-factor of the cavity, the zeroth-order reflection of the grating was used as an output coupler. Note that even with this scheme, only sequence lines with a high rotational quantum number ($j > 21$) were observed. This is a result of the frequency separation between adjacent CO_2 regular band and sequence band transitions increasing with rotational quantum number j such that the nearby regular band transition dominates lasing within the cavity for low j sequence band transitions. The probe pulse was sent through the optically pumped CO_2 cell in a double-pass scheme with the rightmost dichroic mirror used for reflection. A 50/50 beam-splitter directed the reflected pulse into a HgCdTe signal detector for measurement. Time-resolved gain could then be determined from comparison of the temporal profiles of the probe pulse and pump pulse, and, thus, time-resolved measurements of T_3 and T were obtained using the methods described previously in Chapter 2.

For the high-pressure measurements of gain lifetime discussed in Chapter 4.4, where precise tunability was no longer required, the intra-cavity grating was removed from the probe laser cavity and a 50% reflective mirror was used as an output coupler. To prevent cross-interaction between the pump and probe laser, the probe beam was aligned through the cell and reflected off the right dichroic mirror at a slight angle, measuring gain in a V-shaped double-pass scheme.

4.1 Low-pressure lasing

Our first experimental results were the demonstration of efficient lasing in an optically pumped CO_2 active medium at low pressures. Figure 9(a) shows the 10 μm energy generated from lasing in a cell containing 35 Torr of pure CO_2 optically pumped by ~2 mJ pulses generated by the Fe:ZnSe master oscillator. Here, the 97.7% reflective diffraction grating was used as an output

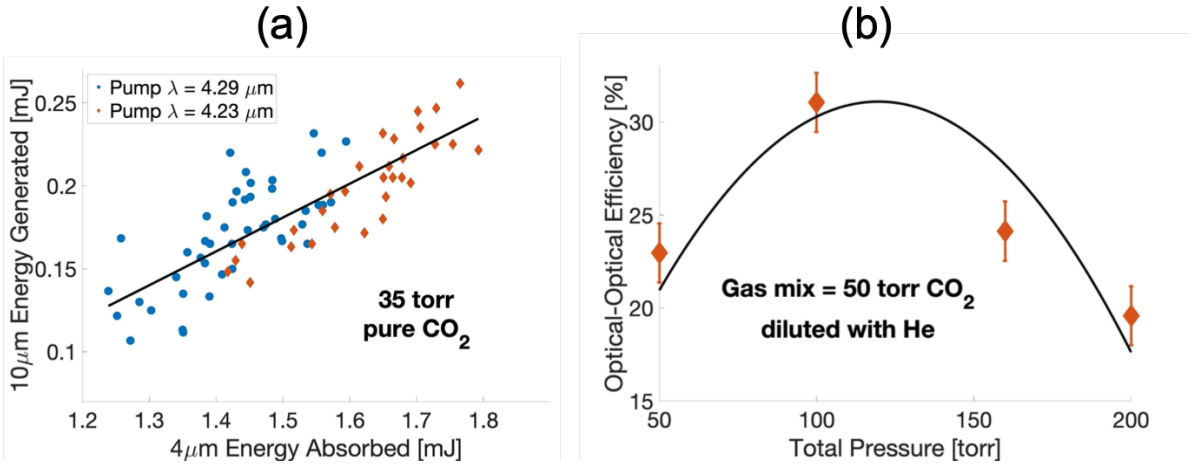

Figure 9. (a) The amount of 10 μm energy generated in the optically pumped CO_2 laser as a function of absorbed pump energy. A least squares linear fit to the aggregate data is shown in black. (b) Optical-to-optical conversion efficiency in the optically pumped CO_2 laser for a pump wavelength of 4.23 μm. The black curve indicates a least squares parabolic fit to the data.

coupler in place of the second dichroic mirror shown in Figure 8. The ~4.3 μm pump pulse energy was measured before the cell using the reflection off of the NaCl wedge and after the cell by measuring the pump energy reflected off of this diffraction grating. Blue dots correspond to lasing output when the pump laser was tuned to 4.29 μm, the peak of the 4P branch of the CO_2 absorption spectrum. Red dots correspond to a pump wavelength of 4.23 μm, the peak of the 4R branch, where absorption is naturally higher, allowing for more efficient pumping. A linear slope can be seen with no indication of pump energy saturation. Figure 9(b) shows the optical-to-optical conversion efficiency of 4.23 μm pump energy to 10.6 μm lasing energy as a function of total pressure in mixtures of 50 Torr of CO_2 and ballast He. A peak conversion efficiency of >30% was measured, nearing the theoretical quantum limit of ~40%.

Using this diffraction grating as an output coupler, lasing was not observed at pressures >1 atm. Using a second identical dichroic mirror to maximize the Q-factor of the cavity, however, allowed for the observation of lasing at total pressures up to 3 atm (50 Torr CO_2 diluted with He).

At such pressures, the collisional broadening of rovibrational lines resulted in stronger absorption of the pump energy, and it was thus necessary to tune the pump wavelength along the high-*j* transitions of the 4P absorption branch to ~4.35 μm, where absorption is significantly lower. Stable lasing also required a precise tuning of the pump laser wavelength on the line center to avoid resonant nonlinear optical effects in CO_2, as self-focusing and -defocusing of the pump beam were observed when pumping CO_2 on the red side and the blue side of resonant rovibrational transitions, respectively [29]. It was discovered that both of these nonlinear effects negatively impacted the efficiency of the optically pumped CO_2 laser, and a cylindrical "pencil-like" pump beam was optimal.

Prior to the development of the MOPA system, the pump pulses provided by the master oscillator were limited to energies of ≤2.5 mJ, and it was estimated that this lack of pump energy limited the observation of high gain and lasing at pressures above 3 atm. To confirm this hypothesis, a more detailed study of the gain dynamics in optically pumped CO_2 was then carried out, which will be described in the following section.

4.2 Gain dynamics

As detailed in Chapter 2, the distribution of population and thus the gain dynamics of an excited CO_2 medium can be accurately described using a temperature model [20,21]. Knowledge of temperature kinetics is critical for laser optimization, and experimentally observed molecular kinetics in CO_2 lasers have been shown to deviate considerably from theoretical modeling, especially at high levels of vibrational excitation [20,23]. To study this, we performed small-signal gain measurements on different rovibrational lines of the CO_2 gain spectrum to experimentally

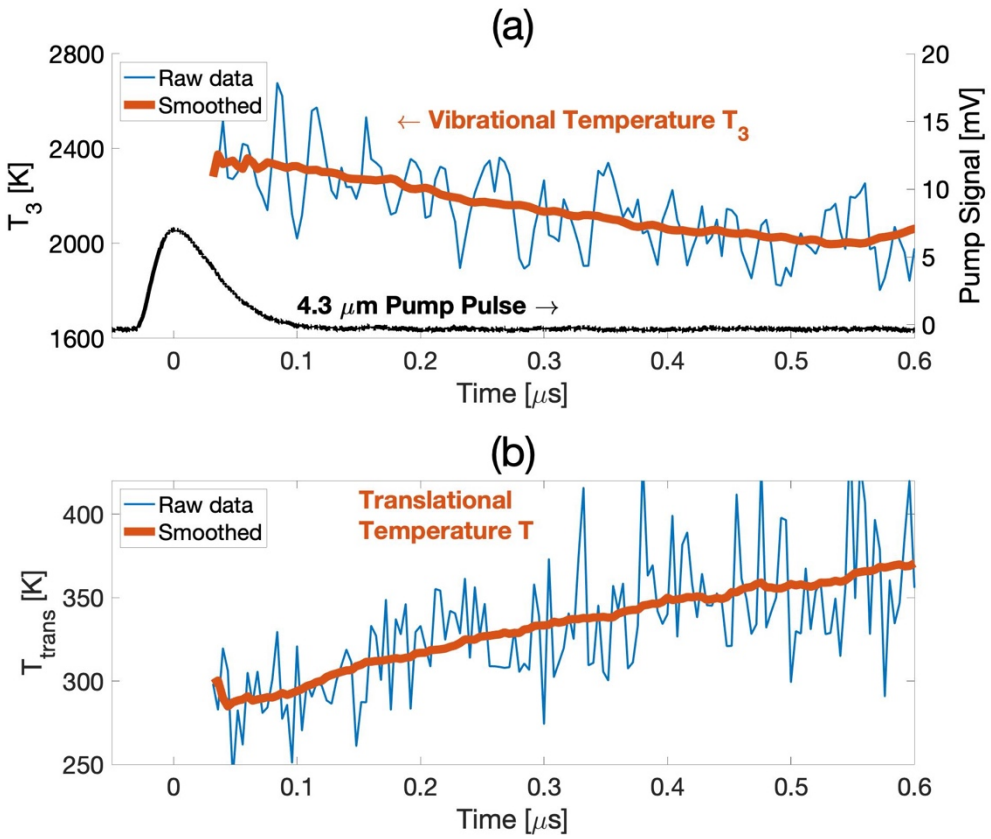

Figure 10. (a) The asymmetric stretching mode vibrational temperature T_3 and (b) the translational temperature T within a cell of 50 torr pure CO_2 optically pumped at 4.3 μm as a function of time. The blue curves show the results of raw data; the red curves show this data with a 50 point moving average filter applied to reduce noise. The pump pulse temporal profile is shown in black.

measure the vibrational temperature, T_3, and the rotational temperature, T, as a function of time in a CO_2 cell optically pumped at ~4.3 μm using the methods described in Chapter 2 [15].

Figure 10 shows the results of these measurements for an active medium of 50 torr pure CO_2 pumped at 4.29 μm. Asymmetric stretching mode vibrational temperature, T_3, and translational temperature, T, are shown as a function of time. It can be seen that almost immediately after the absorption of the pump pulse (at time t = 0), a peak T_3 value of ~2400 K is reached, while translational temperature is measured to be near room temperature (~300 K) as expected. This T_3 value corresponds to a record-high peak gain coefficient of ~30%/cm. Note that

a TEA CO_2 laser pumped by electric discharge rarely achieves a T_3 value above ~1800 K or gain coefficients above 2-3%/cm [18]. Even optimized, non-self-sustained discharge-pumped CO_2 systems are typically only capable of reaching gain coefficients of 4-6%/cm. The asymmetric stretching mode then collisionally relaxes and energy is redistributed to other modes, resulting in a decrease in T_3 and an increase in T as shown in Figure 10. It should be noted the observation of gain on a sequence band transition (002-101), which was required for this measurement of T_3, immediately after pumping gives further confirmation that the asymmetric stretching mode reaches equilibrium before the gas mixture as a whole.

These measurements were repeated for various CO_2-He mixtures to determine the effect of adjusting total pressure and CO_2 concentration on peak values of T_3. Large T_3 values were only obtained in mixtures with small amounts of CO_2 gas, again indicating that greater pump energy is required to obtain high T_3 values in a larger partial pressure of CO_2. To study the scalability of this system to the high pressures required for sub-picosecond pulse amplification, theoretical calculations were performed to estimate the 4.3 μm pump energy required to achieve high gain in CO_2 at different pressures. Figure 11 shows theoretical calculations for the vibrational temperature, T_3, and the corresponding peak gain coefficient as a function of absorbed energy per unit volume for various amounts of pure CO_2 gas. The pump energy is assumed to be entirely deposited into the asymmetric stretching mode, resulting in the following equation relating T_3 and absorbed pump energy [23]:

$$E_{abs} = \frac{N_{CO_2}(\sum_{v=1}^{9} E_v N_v)}{\sum_{v=0}^{9} N_v}$$

where N_{CO_2} is the total number density of CO_2 molecules, E_v is the energy of the $00v$ vibrational state, and N_v is the population of this state (see Equation 2 in Chapter 2). The diamond markers in Figure 11 indicate experimentally measured T_3 values and their corresponding peak gain coefficients. It is estimated that nearly all of the pump energy is absorbed in the cell in the 200 torr case, corresponding to an absorbed energy per volume of ~60 mJ/cc. It is thus apparent that a much greater amount of pump energy is required to achieve T_3 > 2000 K in more than 50 torr CO_2 due to simple conservation of energy. The lack of absorbed energy in the 10 torr case is attributed to the extremely small width of the 4.3 μm CO_2 absorption spectral lines at such low pressures in comparison with the ~2 nm bandwidth of the 4.3 μm pump laser.

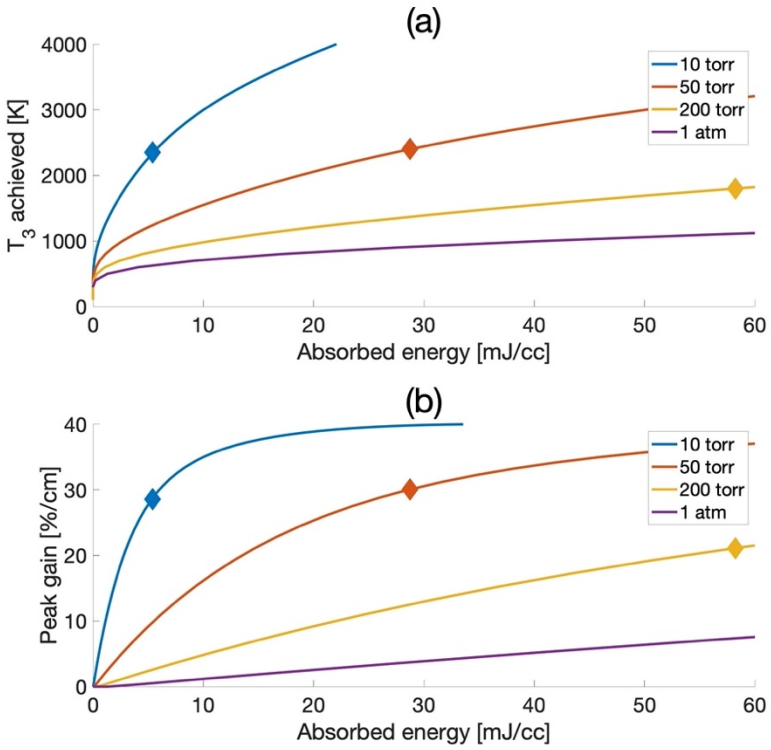

Figure 11. (a) The asymmetric stretching vibrational mode temperature T_3 and (b) the corresponding peak gain coefficient in an optically pumped CO_2 active medium vs. absorbed 4.3 μm pump energy per volume. Each color corresponds to a different amount of pure CO_2. Experimental measurements are shown in diamonds.

To further investigate gain limitations in an optically pumped CO_2 system, measurements were performed in mixtures where the concentration of CO_2 is heavily diluted with Helium. Note that adding He serves two purposes, as it both collisionally broadens the CO_2 lines and efficiently removes heat deposited in the gas. Figure 12 shows experimental measurements of peak T_3 as a function of pressure in pure CO_2 (blue curve) and in CO_2-He mixtures containing a constant 10 torr of CO_2 and ballast He (red curve). It is clear that increasing the amount of CO_2 reduces T_3 for the reasons discussed above. It is also evident, however, that increasing the amount of Helium while maintaining constant partial pressure of CO_2 increases T_3. This result is attributed to increased absorption of 4.3 μm pump energy due to the broadening of spectral lines via CO_2-He collisions. These results give further evidence that very high vibrational temperatures can be achieved in a CO_2 system optically pumped by Fe:ZnSe laser pulses, but a multi-atmosphere CO_2 laser requires a much more energetic pump source.

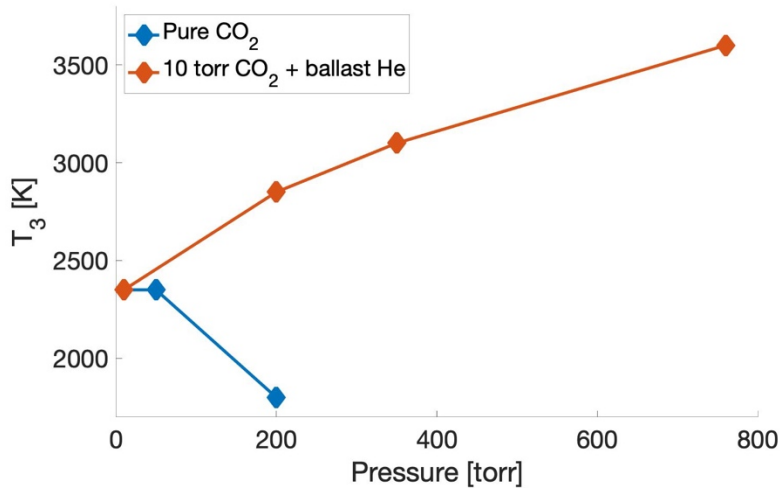

Figure 12. The peak asymmetric stretching vibrational mode temperature, T_3, in an optically pumped CO_2 active medium as a function of total pressure for pure CO_2 (see blue curve) and for dilute CO_2 mixtures (see red curve).

4.3 High-pressure lasing

The development of the Fe:ZnSe MOPA capable of producing ≤60 mJ pulses allowed us to confirm whether increased pump energy could result in gain at high pressures. In addition, the tunability of the Fe:ZnSe pump laser allowed us to study the effects of varying absorption within the CO_2 active medium by changing the wavelength of the pump pulse. Again, lasing was studied using the experimental setup depicted previously in Figure 8. A 6 cm cell was filled with various mixtures of CO_2 and Helium gas and pumped at several different wavelengths with the objective of observing lasing at the highest possible total pressure.

Figure 13(a) shows the normalized absorption spectrum at ~4.3 μm for a mixture of 0.75 atm CO_2 and 9.25 atm Helium, which was close to the optimal ratio as will be discussed below. It can be seen that varying the wavelength of the continuously tunable Fe:ZnSe pump laser along this CO_2 absorption spectrum can give access to a broad range of absorption values. The red markers in Figure 13(a) indicate the five pump wavelengths studied in this experiment, ordered from maximum (~3.5 cm^{-1}) to minimum (~0.2 cm^{-1}) absorption. Wavelengths were chosen to study a range of absorption from the peak to the wing of the distribution, and 4.256 μm (marker 2 in Figure 13(a)) was chosen specifically because it corresponds to the fourth sub-harmonic of the wavelength of a Nd:YAG laser (1064 nm), a possible alternative pump source [30,31].

Figure 13(b) displays the maximum total pressure at which lasing was observed as a function of measured absorption coefficient for a cell filled with different partial pressures of CO_2 and ballast He. The numbers next to each marker indicate the corresponding pump wavelength as shown in Figure 13(a), and the dashed lines indicate a calculated absorption coefficient that would correspond to 50% and 99% of the pump energy being absorbed over the 6 cm cell length. Note that for each of the markers to the right of the second dashed line, the entire pump pulse energy

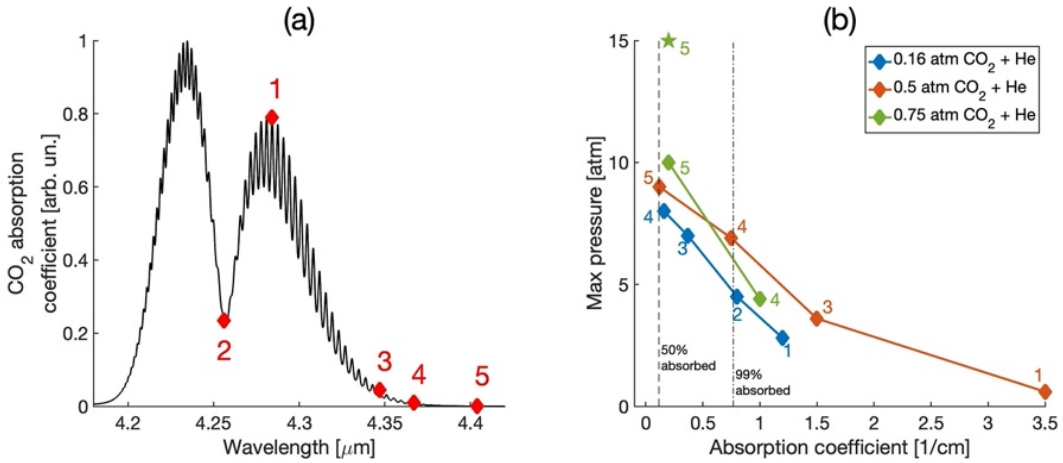

Figure 13. (a) Normalized absorption in 0.75 atm CO_2 and 9.25 atm He. Red markers indicate pump wavelengths used in experiment. (b) Maximum lasing pressure vs estimated experimental absorption coefficient. Numbers correspond to pump wavelengths indicated in (a). The green star indicates maximum lasing pressure after increasing the pump intensity by a factor of ~2 to ~5.3 MW/cm^2.

was absorbed. It can be seen that tuning the pump wavelength far from the peak of the absorption spectrum was necessary to achieve lasing at high pressures. This is attributed to the fact that in high absorption mixtures, nearly all of the pump energy was absorbed over a short distance, reducing the gain length of the CO_2 active medium. Increasing the partial pressure of CO_2 allowed for increased gain coefficients, but this also increased absorption and thus reduced the gain length. Note that lasing was not achieved at pressures above 5 atm when the cell was pumped at 4.256 µm. The relatively high absorption coefficient here dictates that, if using an alternate pump source limited to this wavelength, efficient short pulse amplification will require cell length optimization or utilizing a transverse pump configuration.

For high-pressure lasing in a 6 cm cell, the optimal partial pressure of CO_2 was found to be 0.75 atm and the optimal pump wavelength was found to be 4.40 µm. Further focusing of the pump beam to increase the intensity by a factor of ~2 to ~5.3 MW/cm2 allowed for the achievement of lasing at total pressures up to 15 atm, as indicated by the green star in Figure 13(b).

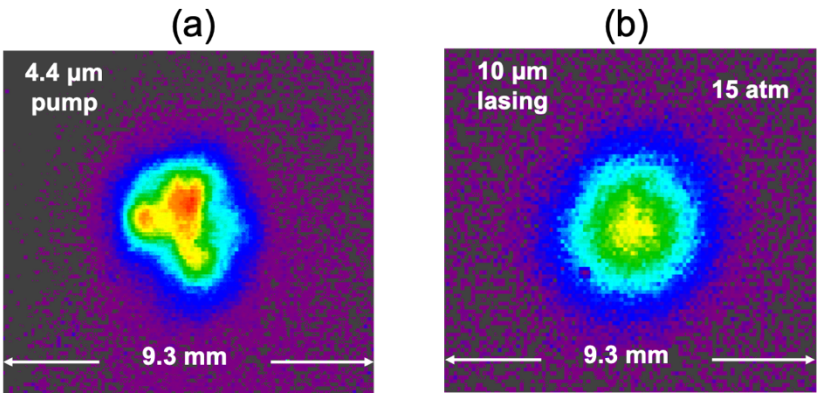

Figure 14. Beam profiles of (a) the 4.4 μm pump laser and (b) the 10.6 μm optically pumped CO_2 laser output at a total pressure of 15 atm.

Typical spatial beam profiles of the Fe:ZnSe pump pulse and the 10.6 μm optically pumped CO_2 laser pulse are shown in Figure 14. Note that the maximum pressure in this experiment was ultimately limited by the gas handling system, and higher pressures can be reached with further optimization. In addition to advantageously increasing the absorption length in the cell, pumping this far from the peak of absorption eliminates the need for purging the experimental area with Ar or N_2, as CO_2 absorption in the ambient air at a wavelength of 4.40 μm is negligible. It should also be noted that the experimentally measured absorption using high intensity, 4.40 μm radiation was significantly higher than that theoretically predicted using HITRAN molecular constants [32]. This can be attributed to the fact that, within the cell, there may be significant absorption on the 001-002 and 002-003 absorption bands, as all vibrational levels in the asymmetric mode are populated and the absorption transitions of these sequence bands are red-shifted due to CO_2 anharmonicity. This may also indicate a non-Boltzmann distribution of population among rovibrational energy levels for highly excited CO_2 molecules and requires further study.

The optical-to-optical conversion efficiency was also measured using several different output couplers with this same optimal CO_2 pressure and pump wavelength. Figure 15(a) shows the conversion efficiency as a function of total pressure for cavities formed by a second dichroic

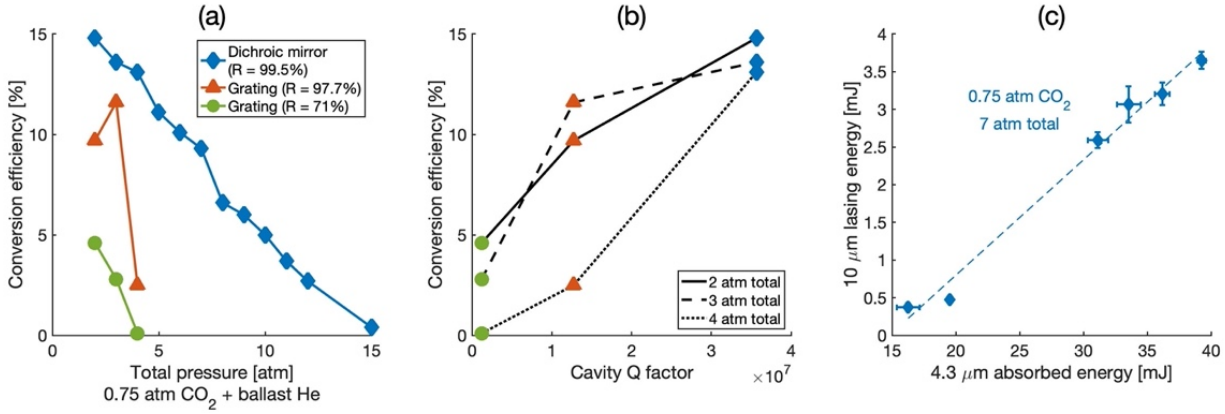

Figure 15. (a) Optical-optical conversion efficiency of the optically pumped CO_2 laser as a function of pressure using three different output couplers. (b) Conversion efficiency as a function of cavity Q factor at three different pressures. (c) 10 μm lasing energy generated vs. 4.40 μm pump energy absorbed at 7 atm total pressure.

mirror, a 97.7% reflective diffraction grating, and a 71% reflective diffraction grating as indicated. It should be noted that flat reflective diffraction gratings were used, while the dichroic mirror had a radius of curvature of 70 cm, which likely helped reduce diffraction losses and therefore the lasing threshold. Figure 15(b) shows the same set of data, here presenting the conversion efficiency as a function of cavity Q factor. It was found that the highest reflectivity output coupler provided the best performance both in terms of maximum achievable lasing pressure and in terms of highest conversion efficiency.

Figure 15(c) shows measurements of 10.6 μm lasing energy as a function of absorbed 4.40 μm energy at a total pressure of 7 atm for the cavity utilizing a second dichroic mirror as an output coupler. Note that for this measurement, the range of absorbed energy was controlled not by tuning wavelength but by attenuating the pump pulse energy by a factor of 2, and small variations in the data reflect the day-to-day change of the output of the Fe:ZnSe pump laser. There is no sign of

saturation with increased pump energy, indicating the potential for scaling 10 µm output to higher energies.

4.4 Gain lifetime

Small-signal gain measurements were also performed to study the gain lifetime of an optically pumped CO_2 active medium. Relaxation rates have previously been measured in CO_2 systems pumped at ~4.3 µm [33,34]. However, the extreme excitation of the CO_2 asymmetric stretching mode that is presented in this study may lead to different relaxation rates and has not been tested experimentally. To study this, small-signal gain and gain lifetime were measured by probing an optically pumped CO_2 system in the V-shaped double-pass scheme described previously [16].

Figure 16 shows a typical measurement of the 4.40 µm pump pulse (in blue) and the total amplification factor of the 10.6 µm probe pulse (in red) as a function of time for an example gas mix of 0.75 atm CO_2 and 10.25 atm He. It can be seen that, even at 11 atm, amplification reaches a maximum after the termination of the pump pulse, indicating the importance of repopulating the

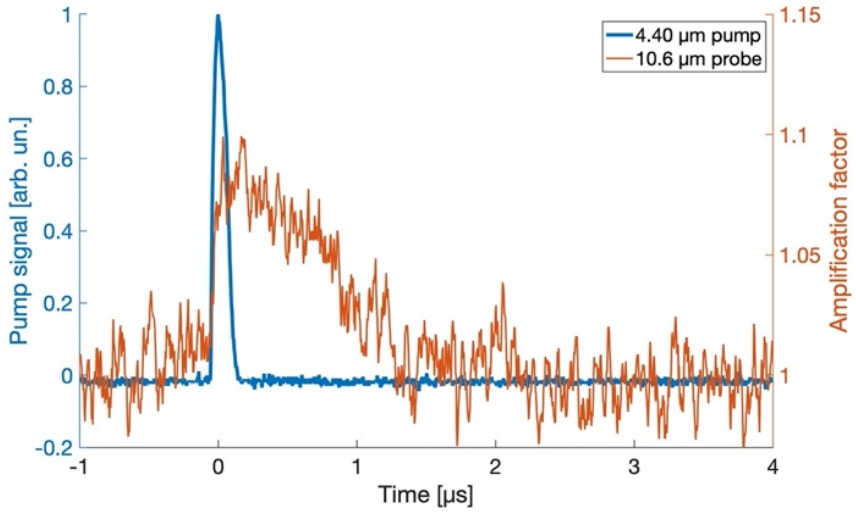

Figure 16. The 4.40 µm pump pulse (blue) and the amplification factor of the 10.6 µm probe pule (red) as a function of time for a gas mix of 0.75 atm CO_2 and 10.25 atm Helium.

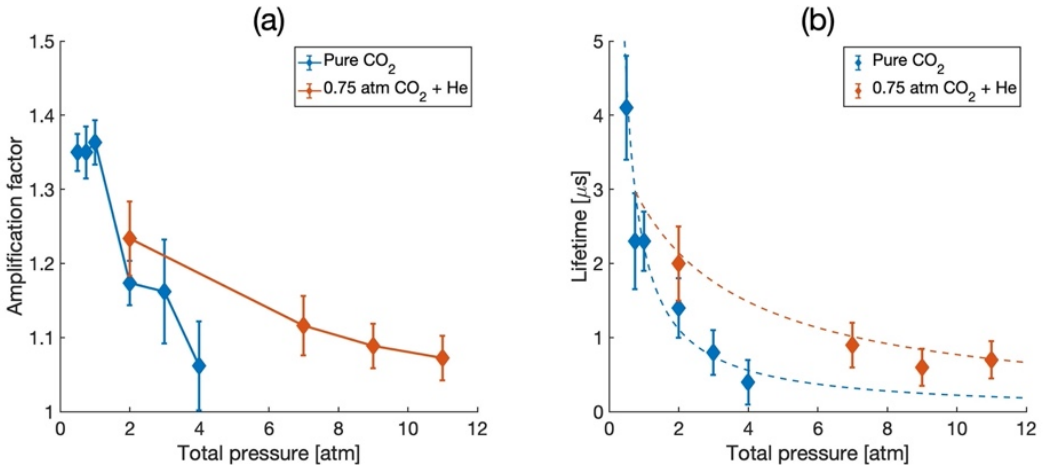

Figure 17. (a) Total amplification of the 10.6 μm probe pulse in the 6 cm optically pumped CO_2 cell and (b) gain lifetime as a function of total pressure.

upper laser level 001 by intramode collisional energy exchange to reach the maximum gain coefficient. Figure 17(a) shows the peak of this total amplification factor as a function of pressure. The blue and red curves correspond to measurements made in pure CO_2 and in 0.75 atm CO_2 mixed with ballast He, respectively. Fitting an exponential curve to the decay of these measured gain signals over time resulted in the measured gain lifetimes displayed in Figure 17(b). The dashed lines in Figure 17(b) correspond to values calculated using the experimentally determined relaxation rates for CO_2-CO_2 and CO_2-He collisions measured by Inoue et. al. and Lepoutre et. al. [33,34]. From the data in Figure 17(b), it is clear that our measured gain lifetimes agree well with these previously published values, indicating that for our pumping conditions, the physical processes occurring in an optically pumped CO_2 active medium do not differ significantly from those published in literature for a lower degree of excitation. Importantly, a long gain lifetime of ~1 μs at high pressures ≥10 atm opens the opportunity for building both regenerative and multi-pass amplifiers suitable for amplifying short seed pulses. Thus, in the direct optical pumping

scheme using 4.4 μm Fe:ZnSe lasers, a high conversion efficiency of ~10% could be reached when the stored energy can be extracted in a short pulse.

4.5 Lasing in indirectly pumped CO_2

Using the ≤60 mJ Fe:ZnSe MOPA system, lasing was also studied in CO-CO_2-He mixtures utilizing the indirect pumping scheme, in which CO molecules are optically excited and energy is collisionally transferred to the CO_2 asymmetric stretching mode and thus the upper laser level (see Figure 2(b)). This scheme is motivated by the potential of further increasing the gain lifetime at high pressures due to the slow exchange of vibrational energy in a dual molecular system where the absorbing two-atomic molecule has a long relaxation time [12]. This scheme may also be used to avoid deleterious nonlinear refraction that can occur in CO_2 [29], which has a dipole moment three times larger than that of CO.

The same setup illustrated in Figure 8 was used for these measurements, with the Fe:ZnSe pump laser wavelength now tuned to ~4.6 μm to coincide with absorption in the 0-1 vibrational band of CO. Figure 18(a) shows the normalized absorption spectrum of 1 atm CO, and the red markers indicate the pump wavelengths used in this experiment. Figure 18(b) shows the maximum total pressure at which 10.6 μm lasing was analyzed for two different gas mixtures as shown. The two dashed lines again indicate the absorption coefficients at which 50% and 99% of the pump pulse energy are absorbed over a length of 6 cm, and all pump energy was absorbed for the rightmost two data points. Note that lasing at pressures above 4 atm was not achieved in either the 9:1 CO_2:CO or the 10:3:27 CO_2:CO:He mixes, and varying the absorption by tuning pump wavelength did not have an observable positive effect on the maximum lasing pressure. While we have indeed observed a gain lifetime that is several times longer than that for direct pumping, the

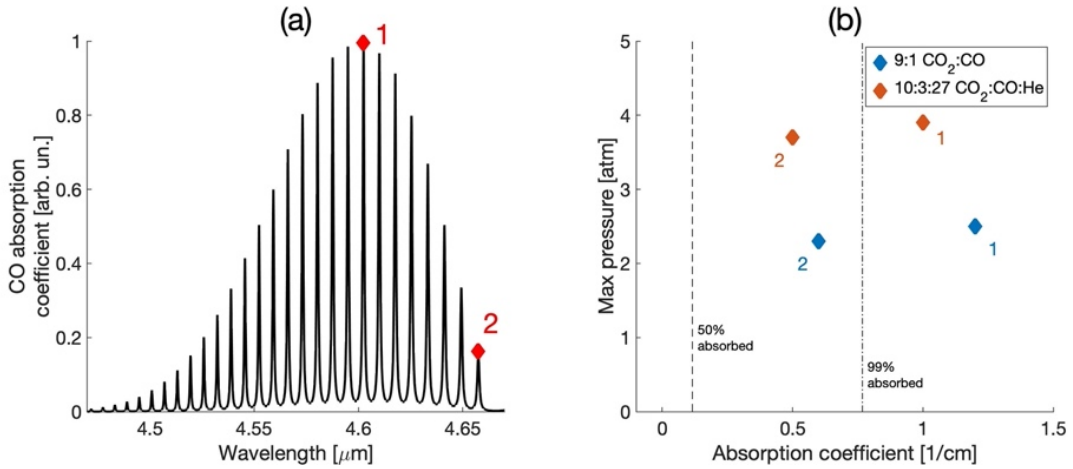

Figure 18. (a) Normalized absorption in 1 atm CO. Red markers indicate pump wavelengths used in experiment. (b) Maximum lasing pressure vs estimated experimental absorption coefficient. Numbers correspond to pump wavelengths indicated in (a).

gain values and 10 μm output stability were clearly inferior to those measured in the case of 4.4 μm pumping of the CO_2 medium.

For both mixtures, an audible noise corresponding to heat or pressure waves inside the cell could be heard upon the arrival of the pump pulse. The gas mixtures were flowed slowly through the cell to reduce the effects of this, but these pressure waves can play a significant role in vibrational energy exchange processes, thus hindering the performance of indirectly pumped CO_2 laser and limiting the maximum total pressure to <4 atm in this experiment. A fast flow of the gas should be able to mitigate this effect, but extra modifications were beyond the scope of our study.

4.6 Possibility of repetition rate scaling

While all the measurements above using the full Fe:ZnSe MOPA system have been conducted at a relatively low repetition rate of 3 Hz, it is important to identify the rate at which the gas molecules in the system recover from the disturbance of pressure waves caused by the absorption and

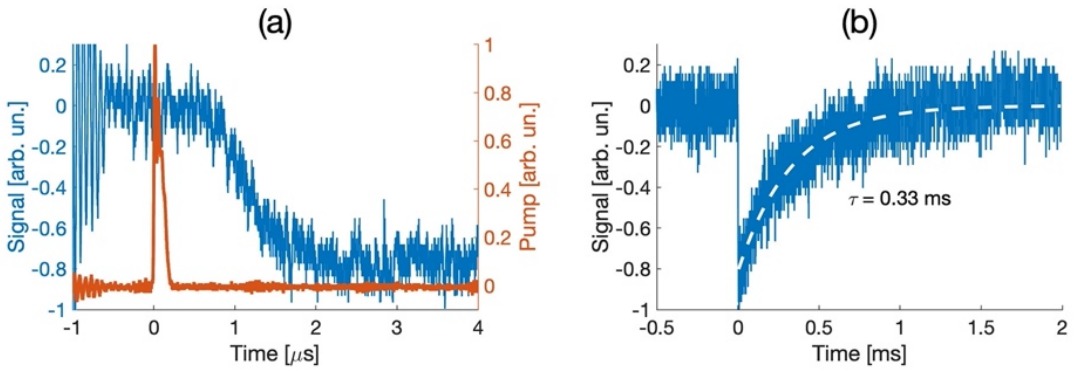

Figure 19. (a) Deflected probe signal (in blue) and Fe:ZnSe pump pulse (in red). (b) Deflected probe signal and recovery. The dashed white line indicates an exponential fit with a time constant of 0.33 ms.

dissipation of heat caused by the energetic pump pulse. To do this, we used a visible cw He-Ne probe laser to analyze how quickly the refractive index of the gas recovers after absorption of the pump pulse. Figure 19 indicates the results of these red beam deflection measurements in a gas mixture of 0.75 atm CO_2 and 9.25 atm He pumped at 4.4 μm.

Figure 19(a) shows the probe signal in blue and the Fe:ZnSe laser pump pulse in red on a microsecond time scale. It can be seen that immediately after the ~200 ns pump pulse, the probe signal remains unaffected, but ~1 μs after the pump pulse, the probe beam is deflected, and the signal is reduced. Figure 19(b) shows the recovery of the probe signal for a similar pump pulse energy on a longer time scale. It can be seen that after ≥1 ms, the gas system has returned to equilibrium and the visible probe signal returns to the initial value. Fitting an exponential curve gives a relaxation time constant of ~0.33 ms at this 10 atm total pressure. A similar result was measured in CO-CO_2 mixes, where the relaxation time constant was measured to be ~0.50 ms in a mix of 1 atm CO, 0.1 atm CO_2, and 8.9 atm He. Given that this relaxation time is inversely proportional to pressure, it can be estimated that for the high pressures (>10 atm) desirable for short-pulse amplification, the system will reset in ≤1 ms. This indicates that an optically pumped CO_2 laser system is capable of operating at a repetition rate of ~1 kHz.

There are currently two feasible options for the development of a 1 kHz solid-state source capable of pumping a CO_2 active medium for the amplification of 10 μm pulses to GW level powers (with a few mJ in a few ps). A 1 kHz Fe:ZnSe laser system pumped by Er:YAG lasers providing mJ-level output has already been developed and could be scaled to provide tens of mJs utilizing commercially available 50 mJ, 1 kHz Er:YAG lasers for pumping [13]. Alternatively, the efficient frequency down-conversion of 1064 nm Nd:YAG laser pulses could be used to generate pulses at 4.256 μm, the fourth sub-harmonic of this wavelength. Nd:YAG lasers are capable of operating at a kilohertz repetition rate, and efficient conversion of 15 ns pulses from 1064 nm to 2128 nm and from 2.1 μm to ~3-5 μm has already been demonstrated with optical parametric oscillators operating at or near the degeneracy point [30,31]. It should be noted that for such a CO_2 laser system producing multi-watt average powers, a certain heat exchanger similar to that used in industrial CO_2 pulsed lasers should be designed and utilized.

5 Simulation results

The demonstration of lasing and gain at high pressures up to 15 atm indicate that an optically pumped CO_2 amplifier can achieve a broad bandwidth capable of amplifying picosecond or sub-picosecond pulses. Historically, however, the interest in high-pressure, optically pumped, compact CO_2 lasers was motivated by the prospect of continuous spectral tuning, and thus the experimental realization of amplifying short pulses in such a medium has never been performed or even analyzed numerically. Recently, we have shown a path towards achieving high peak powers in 10 μm pulses by the direct amplification of a 3 ps pulse and the chirped-pulse amplification of a 1 ps pulse in a CO_2 amplifier pumped by a tunable 4.3 μm pump source using numerical simulations [17]. These

simulations were performed using the *co2amp* software program, which is based on density matrix formalism and analyzes broadband pulse amplification in a CO_2 active medium [35].

As discussed in Chapter 1, pressure broadening allows the CO_2 gain spectrum to reach a bandwidth of ~1 THz (FWHM) for the amplification of short pulses (see Figure 1). Gain narrowing limits the minimum pulse duration to ~3 ps [6], but by introducing CO_2 isotopologues with frequencies that are slightly shifted from that of the regular $^{12}C^{16}O_2$ molecule, it is possible to further increase the bandwidth of the CO_2 gain spectrum to realize the amplification of even shorter pulses. Adding the $^{13}C^{16}O_2$ isotopologue into the active medium extends the bandwidth due to the overlap between the $^{12}C^{16}O_2$ 10P branch with the $^{13}C^{16}O_2$ 10R branch [36]. Numerical optimization of the ratio between $^{12}C^{16}O_2$ and $^{13}C^{16}O_2$ in a gas mix of 1 atm total CO_2 and 19 atm He was performed to provide an approximately constant gain over a >1 THz bandwidth. The resulting mix consisted of 63% $^{12}C^{16}O_2$ and 37% $^{13}C^{16}O_2$. Figure 20(a) shows the calculated gain profile of such a laser mix optically pumped to a vibrational temperature, T_3, of 3300 K. Note that

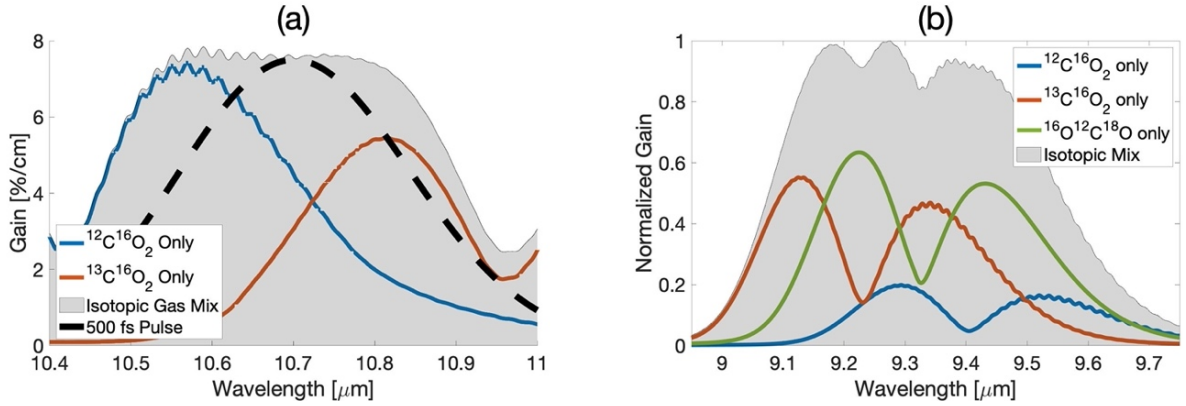

Figure 20. (a) The gain spectrum of an active medium comprised of 1 atm CO_2 (63% $^{12}C^{16}O_2$ isotopologue, 37% $^{13}C^{16}O_2$) and 19 atm He, pumped to a T_3 value of 3300 K. The dashed black line shows the frequency spectrum of a 500 fs seed pulse centered at 10.7 um. (b) The normalized gain spectrum of an active medium comprised of 1 atm CO_2 (21% $^{12}C^{16}O_2$, 43% $^{12}C^{18}O_2$, and 36% $^{12}C^{16}O^{18}O$ isotopologue) and 19 atm He. A total bandwidth of ~3 THz centered around 9.3 μm wavelength is achieved.

regardless of which CO_2 isotopologue absorbs the pump radiation, near resonant interactions between the upper laser levels of the two CO_2 isotopologues quickly establish equilibrium between these levels, ensuring that a single vibrational temperature, T_3, can be applied to both isotopologues. Later, in section 5.2, we will show the results of simulations describing the amplification of a 0.5 ps pulse in a gas mix with the gain spectrum presented in Figure 20(a).

Amplification of sub-picosecond (0.3-0.5 ps) pulses requires further broadening of the gain spectrum. The necessary bandwidth can be achieved, for example, around 9 μm wavelength with the $^{12}C^{18}O_2$ and $^{12}C^{16}O^{18}O$ isotopologues. Figure 20(b) shows the normalized gain spectrum of a mix of 1 atm CO_2 isotopologues and 19 atm He. An optimized ratio of 21% $^{12}C^{16}O_2$, 43% $^{2}C^{16}O^{18}O$, and 36% $^{12}C^{18}O_2$ was used. It should be noted that while this particular gain spectrum was not used in the simulations discussed in this thesis, a similar mixture of CO_2 isotopologues at lower pressures (~10 atm) was recently used to amplify 9.2 μm, 2 ps pulses to the multi-TW level at Brookhaven National Laboratory [7].

Two simulations are presented in this chapter, both targeting the achievement of GW-level peak powers. The first considers the direct amplification of a 3 ps pulse, while the second considers the chirped-pulse amplification (CPA) of a shorter, sub-picosecond pulse. CPA reduces the intensity of the pulse via stretching before amplification, keeping the intensity of the pulse below the damage threshold of optical elements. CPA is considered only for the sub-picosecond pulse, for which a reduction of intensity becomes necessary. A length of 3 ps is chosen for the longer pulse specifically because direct amplification of 3 ps pulses in a high-pressure CO_2 amplifier is possible without measurable pulse broadening [4-6]. Only the $^{12}C^{16}O_2$ isotopologue is considered for this 3 ps pulse amplification, but a mixture of $^{12}C^{16}O_2$ and $^{13}C^{16}O_2$ isotopologues are considered for the case of sub-picosecond amplification (see Figure 20(a)).

Almost all other simulation parameters are kept identical for both cases. The seed pulse has an energy of 10 μJ, chosen to represent a 10 μm pulse energy typically generated by a laser system using optical parametric amplification pumped around 1 μm and difference frequency generation [37]. Amplification occurs in a 10 cm cell filled with 20 atm of CO_2-He (1:19) gas mix. Due to the relatively low gain and short interaction length in a CO_2 gas laser, reaching GW-level power will require the use of a regenerative amplification scheme, so the simulations consider a cell located between two mirrors with 100% reflectivity. Details on the density matrix-based model used for simulations can be found elsewhere [35].

5.1 Direct amplification of a 3 picosecond pulse

The results of a simulation of direct amplification of a 3 ps pulse centered at 10.29 μm are shown in Figure 21. The central wavelength is chosen to correspond to the peak gain of the 10R branch of the CO_2 gain spectrum. At pressures above ~7 atm, the 10R branch is superior to the 10P branch due to the smaller frequency separation between individual rotational lines. The active medium contains 1 atm CO_2 excited such that T_3 = 4200 K and 19 atm He. Figure 21(a) shows the temporal profile of the pulse before and after passing through 80 cm of active medium. Over this length, a 10 μJ pulse is amplified to ~3 mJ, and the pulse length is very slightly increased to 3.1 ps. Figure 21(b) shows pulse energy as a function of amplifier length. The frequency spectrum of the final pulse is not modified, and all of the amplified energy is contained in a close to transform-limited pulse.

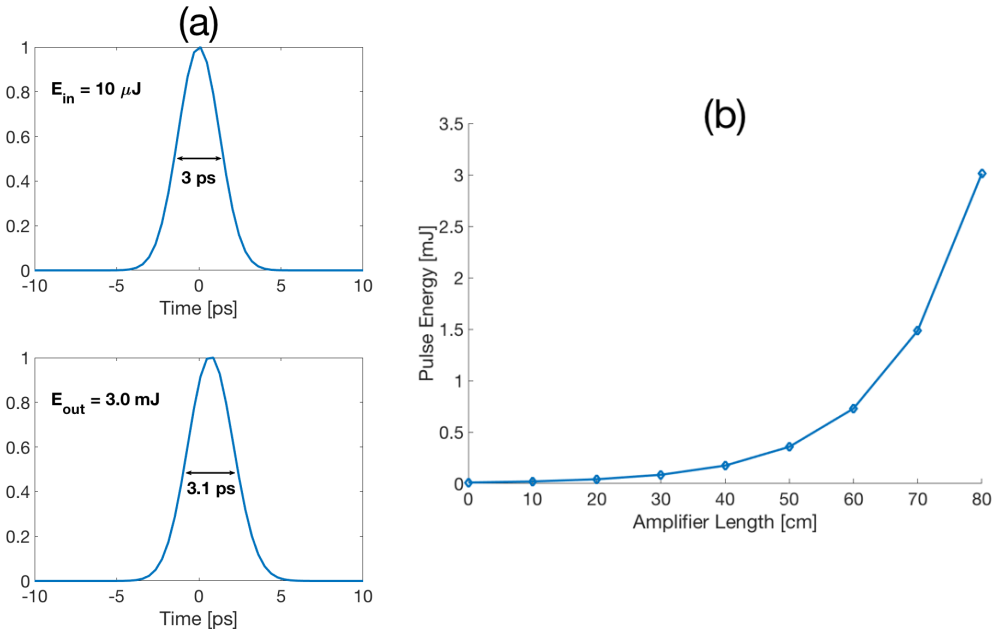

Figure 21. Simulation results for the amplification of a 3 ps pulse centered at 10.29 μm in a gas mix of 1 atm CO_2 and 19 atm He optically excited to a T_3 value of 4200 K. (a) The temporal profile of the pulse before (top) and after (bottom) amplification. (b) The pulse energy as a function of amplifier length, discounting losses due to propagation or output coupling.

5.2 Chirped-pulse amplification of a sub-picosecond pulse

The next simulation is of the chirped-pulse amplification of a sub-picosecond pulse. As discussed earlier, amplification of a pulse of this short duration requires stretching and compressing it to avoid the damage of optical elements due to the high intensity of this pulse and to increase efficiency of interaction in a cm-scale cell. For this simulation, a 0.5 ps input pulse is considered. The pulse is stretched to 160 ps, amplified, and then compressed. A loss of 50% during compression is assumed. The amplification of sub-picosecond pulses requires gain tailoring of the active medium, which is done here with the introduction of the $^{13}C^{16}O_2$ isotopologue as described previously. For this simulation, the CO_2 medium is excited to a T_3 value of ~3300 K. The smaller

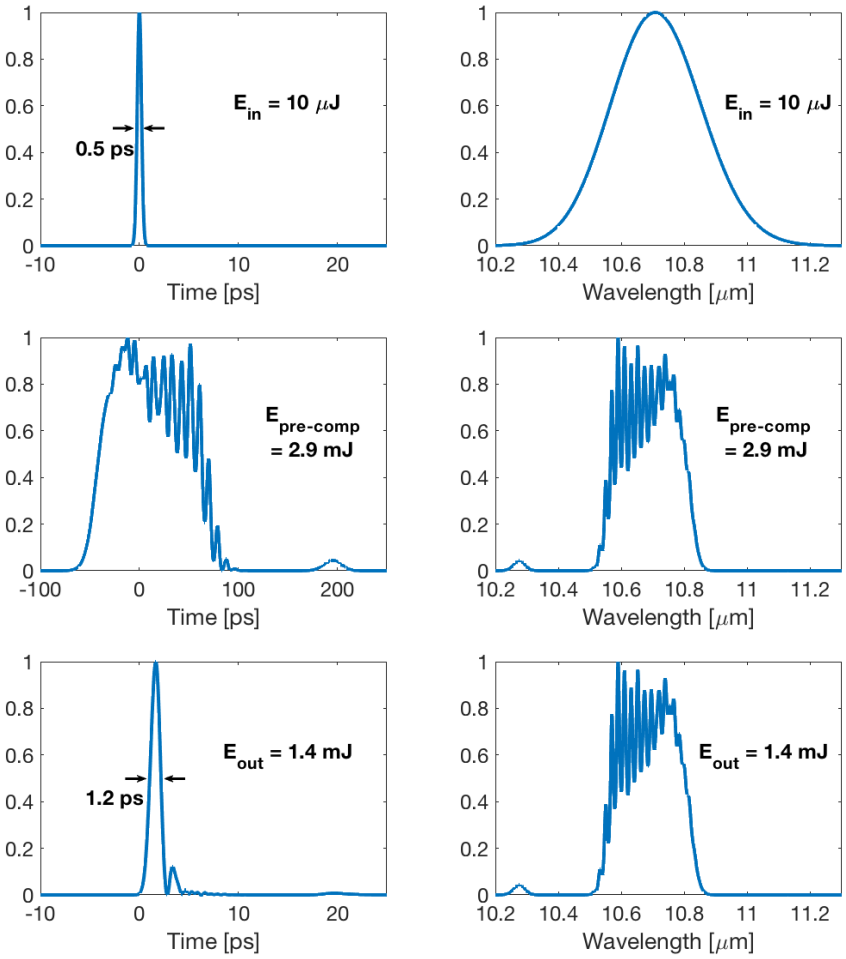

Figure 22. Simulation results for the amplification of a sub-ps pulse in an optically pumped CO_2 amplifier comprised of 1 atm CO_2 (63% $^{12}CO_2$, 37% $^{13}CO_2$) and 19 atm He. The temporal profile of the pulse before stretching (see top), after amplification (see middle), and after compression (see bottom) are shown on the left. The frequency spectrum of the pulse at each stage is shown on the right. 50% loss of energy during compression is assumed.

T_3 value for this gas mix accounts for slightly reduced absorption of the ~4.3 μm pump pulse, a result of the smaller Einstein coefficients of the $^{13}C^{16}O_2$ isotopologue [38].

Figure 22 shows the results of a simulation of CPA of a 10 μJ seed pulse centered at 10.7 μm, where the gain is peaked. The temporal profile and frequency spectrum of the seed pulse before stretching (see top panel), after stretching and amplification (see middle panel), and after

the final compression (see bottom panel) are shown. The imperfect overlap between the frequency spectrum of the pulse and the gain spectrum of the active medium results in a longer final output pulse of 1.2 ps, but this pulse-broadening (gain-narrowing) effect is minimal and still allows for a peak power of 1 GW to be achieved, as a pulse energy of 1.4 mJ is reached after accounting for losses during compression. It is thus demonstrated that a 10 μJ, 0.5 ps pulse can be amplified to GW-level power used chirped-pulse amplification in an optically pumped CO_2 cell containing both $^{12}C^{16}O_2$ and $^{13}C^{16}O_2$ molecules.

6 Conclusion

In this thesis, lasing and gain dynamics are studied in a CO_2 active medium optically pumped at ~4.3 μm for the first time using a tunable Fe:ZnSe laser. When ~2 mJ pump pulses are used, optical-to-optical conversion efficiencies as high as 30% are demonstrated in a low-pressure (<1 atm) optically pumped CO_2 laser. The asymmetric stretching mode vibrational temperature, T_3, and translational temperature, T, are measured as a function of time; T_3 values as high as 3600 K are measured in dilute CO_2 mixtures at a total pressure of 1 atm, and record peak gain coefficients of ~30%/cm are detected in 50 torr of pure CO2.

The use of a more energetic Fe:ZnSe MOPA system as a pump source allowed for 10 μm lasing at total pressures up to 15 atm. It is experimentally demonstrated that tuning the pump wavelength to reduce the absorption coefficient is critical for the achievement of lasing at high pressures, and an optimum pump wavelength is found to be 4.40 μm. A high optical-to-optical conversion efficiency of ~10% is measured at 7 atm total pressure, falling to ~5% at pressures

above 10 atm. This efficiency could be further optimized using a two-pass or transverse pumping scheme, as only ~70% of the total pump energy was absorbed at optimal conditions.

Gain lifetime is also measured as a function of pressure, and the ~1 μs lifetime observed at high pressures indicate the feasibility of using optically pumped CO_2 as a multi-pass or regenerative amplifier. Simulations are performed in which a 3 ps pulse and a sub-picosecond pulse is amplified in such a regenerative amplifier to GW-level peak powers. It is shown that gain tailoring with the use of other CO_2 isotopologues can provide the broad bandwidth needed for amplifying sub-picosecond pulses. An alternative pumping scheme in which CO_2 is indirectly excited via pumping a collisional partner molecule CO is also studied, but it is determined that low gain coefficients and the generation of heat or pressure waves within the cell hinder the performance of this method. He-Ne laser probe beam deflection measurements demonstrate that a high-pressure CO_2 laser can be pumped at a maximum repetition rate of ~1 kHz.

Our results at and above 10 atm make a compact, high-pressure optically pumped CO_2 medium a promising candidate for short 10 μm pulse amplification. With the development of even more energetic pump sources at ~4.4 μm and further work on the design optimization, such an amplification scheme may be used to progressively increase the output to TW-level power in a sub-picosecond 10 μm pulse, potentially providing a novel, compact source for high-field science and studies of atmospheric nonlinear optics in the long-wave infrared.

References

1 S. Tochitsky, E. Welch, M. Polyanskiy, I. Pogorelsky, P. Panagiotopoulos, M. Kolesik, E. M. Wright, S. M. Koch, J. V. Maloney, J. Pigeon, and C. Joshi, "Megafilament in air formed by self-guided terawatt long-wavelength infrared laser," Nat. Photonics **13**, 41 (2019).

2 D. Haberberger, S. Tochitsky, F. Fiuza, C. Gong, R. A. Fonseca, L. O. Silva, W. B. Mori, and C. Joshi, "Collisionless shocks in laser-produced plasma generate monoenergetic high-energy proton beams," Nat. Physics **8**, 95 (2012).

3 I. V. Pogorelsky, M. N. Polyanskiy, and W. D. Kimura, "Mid-infrared lasers for energy frontier plasma accelerators," Phys. Rev. Accel. Beams **19**, 091001 (2016).

4 I. Pogorelsky, M. Babzien, I. Pavlishin, D. Stolyarov, V. Yakimenko, P. Shkolnikov, A. Pukhov, A. Zhidkov, and V. Platonenko, "Terawatt CO2 laser: a new tool for strong-field research," Proc. SPIE **6261**, 626118 (2006).

5 P. Corkum, "Amplification of picosecond 10 μm pulses in multiatmosphere CO_2 lasers," IEEE J. Quant. Electron. **21**, 216 (1985).

6 D. Haberberger, S. Tochitsky, and C. Joshi, "Fifteen terawatt picosecond CO2 laser system," Opt. Express **18**, 17865-17875 (2010).

7 M. N. Polyanskiy, I. V. Pogorelsky, M. Babzien, and M. A. Palmer, "Demonstration of a 2 ps, 5 TW peak power, long-wave infrared laser based on chirped-pulse amplification with mixed-isotope CO_2 amplifiers," OSA Continuum **3**, 459 (2020).

8 I. Wieder, "Flame pumping and infrared maser action in CO_2," Phys. Lett. A **24**, 759 (1967).

9 T. Y. Chang and O. R. Wood, "Optically pumped 33-atm CO_2 laser," Appl. Phys. Lett. **23**, 370 (1973).

10 K. Stenersen and G. Wang, "Direct optical pumping of high-pressure CO_2 and N_2O lasers with a pulsed HF pump laser," IEEE J. Quant. Electron. **22**, 2236 (1986).

11 B. S. Alexandrov, A. V. Aresnjev, M. A. Azarov, V. A. Drozdov, J. P. Koretsky, V. I. Mashendzhinov, V. E. Revich, and G. A. Troshchinenko, "Wide-aperture powerful high-pressure CO2 laser with optical pumping," Proc. SPIE **4644**, 301 (2002).

12 H. Kildal and T. F. Deutsch, "Optically pumped gas lasers," in: Tunable lasers and applications, eds A. Mooradian, T. Jaeger, and P. Stokseth (Springer-Verlag, 1976), pp. 367-377.

13 S. B. Mirov, I. S. Moskalev, S. Vasilyev, V. Smolski, V. V. Fedorov, D. Martyshkin, J. Peppers, M. Mirov, A. Dergachev, and V. Gapontsev, "Frontiers of mid-IR lasers based on transition metal doped chalcogenides," IEEE J. Sel. Top. Quant. Electron. **24**, 1601829 (2018).

14 D. Martyshkin, K. Karki, V. Fedorov, and S. Mirov, "Room temperature, nanosecond, 60 mJ/pulse Fe:ZnSe master oscillator power amplifier system operating at 3.8-5.0 μm," Optics Express **29**, 2387-2393 (2021).

15 D. Tovey, J. J. Pigeon, S. Ya. Tochitsky, G. Louwrens, I. Ben-Zvi, C. Joshi, D. Martyshkin, V. Fedorov, K. Karki, and S. Mirov, "Gain dynamics in a CO_2 active medium optically pumped at 4.3 μm," J. Appl. Phys. **128**, 103103 (2020).

16 D. Tovey, J. J. Pigeon, S. Ya. Tochitsky, G. Louwrens, I. Ben-Zvi, C. Joshi, D. Martyshkin, V. Fedorov, K. Karki, and S. Mirov, "Lasing in 15 atm CO_2 cell optically pumped by a Fe:ZnSe laser," accepted for publication in Opt. Express (2021).

17 D. Tovey, S. Ya. Tochitsky, J. J. Pigeon, G. J. Louwrens, M. N. Polyanskiy, I. Ben-Zvi, and C. Joshi, "Multi-atmosphere picosecond CO_2 amplifier optically pumped at 4.3 μm," Appl. Optics **58**(21), 5756 (2019).

18 W. Witteman, The CO2 Laser (Springer-Verlag, 1987).

19 K. Siemsen, J. Reid, and C. Dang, "New techniques for determining vibrational temperatures, dissociation, and gain limitations in CW CO2 lasers," IEEE J. Quant. Electron. **16**, 668 (1980).

20 I. M. Bertel, V. O. Petukhov, B. I. Stepanov, S. A. Trushin, and V. V. Churakov, "Investigation of the vibrational temperature kinetics in a TEA CO2 laser," Sov. J. Quant. Electron. **12**, 1044 (1982).

21 B. F. Gordiets, A. I. Osipov, E. V. Stupochenko, and L. A. Shelepin, "Vibrational relaxation in gases and molecular lasers," Sov. Phys. Usp. **15**, 759 (1973).

22 J. T. Yardley and C. B. Moore, "Intramolecular vibration-to-vibration energy transfer in carbon dioxide," J. Chem. Phys. **46**, 4491 (1967).

23 R. C. Y. Auyeung and J. Reid, "High vibrational temperatures in optically-pumped CO2," IEEE J. Quant. Electron. **24**, 573 (1988).

24 A. G. Maki, C. C. Chou, K. M. Evenson, L. R. Zink, and J. T. Shy, "Improved molecular constants and frequencies for the CO2 laser from new high-J regular and hot-band frequency measurements," J. Mol. Spec. **167**, 211 (1994).

25 R. K. Brimacombe and J. Reid, “Measurements of anomalous gain coefficients in transversely excited CO_2 lasers,” IEEE J. Quant Electron. **19**, 1674 (1983).

26 C. E. Treanor, J. W. Rich, and R. G. Rehm, “Vibrational relaxation of anharmonic oscillators with exchange-dominated collisions,” J. Chem. Phys. **48**, 1798-1807 (1968).

27 V. Fedorov, D. Martyshkin, K. Karki, and S. Mirov, “Q-switched and gain-switched Fe:ZnSe lasers tunable over 3.60-5.15 μm,” Opt. Express **27**(10), 13934-13941 (2019).

28 A. S. Solodukhin, “Hot-cell-free sequence-band CO_2 laser,” J. Modern Opt. **34**, 577 (1987).

29 J. J. Pigeon, D. Tovey, S. Y. Tochitsky, G. J. Louwrens, I. Ben-Zvi, D. Martyshkin, V. Fedorov, K. Karki, S. Mirov, and C. Joshi, “Resonant nonlinear refraction of 4.3-μm light in CO_2 gas,” Phys. Rev. A **100**, 011803(R) (2019).

30 G. Mennerat and P. Kupecek, “High-energy narrow-linewidth tunable source in the mid infrared,” in *Advanced Solid State Lasers*, W. Bosenberg and M. Fejer, eds. Vol 19 of OSA Trends in Optics and Photonics Series (Optical Society of America, 1998), paper FC13.

31 M. W. Haakestad, H. Fonnum, and E. Lippert, "Mid-infrared source with 0.2 J pulse energy based on nonlinear conversion of Q-switched pulses in $ZnGeP_2$," Opt. Express **22**, 8556-8564 (2014).

32 I. E. Gordon, L. Rothman, C. Hill, R. V. Kochanov, Y. Tan, P. F. Bernath, M. Birk, V. Boudon, A. Campargue, K. V. Chance, B. J. Drouin, J. M. Flaud, R. R. Gamache, J. T. Hodges, D. Jacquemart, V. I. Perevalov, A. Perrin, K. P. Shine, M. A. H. Smith, J. Tennyson, G. C. Toon, H. Tran, V. G. Tyuterev, A. Barbe, A. G. Császár, V. M. Devi, T. Furtenbacher, J. J. Harrison, J. M. Hartmann, A. Jolly, T. J. Johnson, T. Karman, I. Kleiner, A. A. Kyuberis, J. Loos, O. M. Lyulin, S. T. Massie, S. N. Mikhailenko, N. Moazzen-Ahmadi, H. S. P. Müller, O. V. Naumenko, A. V. Nikitin, O. L. Polyansky, M. Rey, M. Rotger, S. W. Sharpe, K. Sung, E. Starikova, S. A. Tashkun, J. V. Auwera, G. Wagner, J. Wilzewski, P. Wcisło, S. Yu, and E. J. Zak, “The HITRAN2016 molecular spectroscopic database,” J. Quant. Spectrosc. Radiat. Transfer **203**, 3 (2017).

33 G. Inoue and S. Tsuchiya, “Vibrational relaxation of $CO_2(00^01)$ in CO_2, He, Ne and Ar in the temperature range of 300-140 K,” J. Phys. Soc. Japan **38**(3), 870 (1975).

34 F. Lepoutre, G. Louis, H. Manceau, “Collisional relaxation in CO_2 between 180 and 400 K measured by the spectrophone method,” Chem. Phys. Lett. **48**(3), 509 (1977).

35 M. Polyanskiy, “co2amp: A software program for modeling the dynamics of ultrashort pulses in optical systems with CO_2 amplifiers,” Appl. Optics **54**, 5136-5142 (2015).

36 C. Freed, L. Bradley, and R. O'Donnell, "Absolute frequencies of lasing transitions in seven CO_2 isotopic species," IEEE J. Quantum Electron. **16**, 1195-1206 (1980).

37 D. F. Gordon, V. Hasson, H. von Bergmann, Y. Chen, A. Schmitt-Sody, and J. R. Penano, "Advanced concepts for high-power, short-pulse CO_2 laser development," Proc. SPIE **9835**, 98350Z (2016).

38 V. S. Starovoitov, S. A. Trushin, V. V. Churakov, and V. F. Pivovarchik, "Dipole moments of laser transitions of isotopic carbon dioxide: experiment and theory," J. Quant. Spectroscopy and Radiation Transfer **41**, 153 (1989).